AGU PUBLICATIONS

JGR

Journal of Geophysical Research: Oceans

RESEARCH ARTICLE

10.1002/2013JC009678

Special Section:
Western Pacific Ocean Circulation and Climate

The Southwest Pacific Ocean circulation and climate experiment (SPICE)

A. Ganachaud[1], S. Cravatte[1,2], A. Melet[1,3], A. Schiller[4], N. J. Holbrook[5], B. M. Sloyan[4], M. J. Widlansky[6], M. Bowen[7], J. Verron[8], P. Wiles[9], K. Ridgway[4], P. Sutton[10], J. Sprintall[11], C. Steinberg[12], G. Brassington[13], W. Cai[14], R. Davis[11], F. Gasparin[1,11], L. Gourdeau[1], T. Hasegawa[15], W. Kessler[16], C. Maes[1], K. Takahashi[17], K. J. Richards[6], and U. Send[11]

[1]Institut de Recherche pour le Développement, UMR5566-LEGOS, (IRD-CNRS-CNES-Université de Toulouse-III), Toulouse, France, [2]IRD, BP A5, Nouméa, New Caledonia, [3]NOAA/GFDL, Princeton University, Princeton, New Jersey, USA, [4]Centre for Australian Weather and Climate Research, CSIRO Wealth from Oceans National Research Flagship, Hobart, Tasmania, Australia, [5]Institute for Marine and Antarctic Studies, University of Tasmania, Australia, [6]International Pacific Research Center, University of Hawaii at Manoa, Honolulu, Hawaii, [7]School of Environment, University of Auckland, New Zealand, [8]LGGE, UMR 5183, CNRS, Université de Grenoble, Grenoble, France, [9]Pacific Island Global Ocean Observing System (PI-GOOS), Apia, Samoa, [10]National Institute of Water and Atmospheric Research Limited, Wellington, New Zealand, [11]Scripps Institution of Oceanography, La Jolla, California, USA, [12]Australian Institute of Marine Science, Townsville, Queensland, Australia, [13]Centre for Australian Weather and Climate Research, Bureau of Meteorology, Sydney, Australia, [14]CSIRO Marine and Atmospheric Research, Aspendale, Victoria, Australia, [15]Japan Agency for Marine-Earth Science and Technology, Yokosuka, Japan, [16]Pacific Marine Environmental Laboratory, National Oceanic and Atmospheric Administration, Seattle, Washington, USA, [17]Instituto Geofisíco del Perú, Lima, Perú

Key Points:
- Southwest Pacific WBCs transport large volumes toward the equator and the pole
- Pathways are complex; water properties tend to erode during the transit
- Variations due to seasons, ENSO and the SPCZ modulate the relative WBC strengths

Correspondence to:
A. Ganachaud
Alexandre.Ganachaud@ird.fr

Citation:
Ganachaud, A., et al. (2014), The Southwest Pacific Ocean circulation and climate experiment (SPICE), *J. Geophys. Res. Oceans*, *119*, 7660–7686, doi:10.1002/2013JC009678.

Received 3 DEC 2013
Accepted 5 OCT 2014
Accepted article online 14 OCT 2014
Published online 19 NOV 2014

Abstract The Southwest Pacific Ocean Circulation and Climate Experiment (SPICE) is an international research program under the auspices of CLIVAR. The key objectives are to understand the Southwest Pacific Ocean circulation and the South Pacific Convergence Zone (SPCZ) dynamics, as well as their influence on regional and basin-scale climate patterns. South Pacific thermocline waters are transported in the westward flowing South Equatorial Current (SEC) toward Australia and Papua-New Guinea. On its way, the SEC encounters the numerous islands and straits of the Southwest Pacific and forms boundary currents and jets that eventually redistribute water to the equator and high latitudes. The transit in the Coral, Solomon, and Tasman Seas is of great importance to the climate system because changes in either the temperature or the amount of water arriving at the equator have the capability to modulate the El Niño-Southern Oscillation, while the southward transports influence the climate and biodiversity in the Tasman Sea. After 7 years of substantial in situ oceanic observational and modeling efforts, our understanding of the region has much improved. We have a refined description of the SPCZ behavior, boundary currents, pathways, and water mass transformation, including the previously undocumented Solomon Sea. The transports are large and vary substantially in a counter-intuitive way, with asymmetries and gating effects that depend on time scales. This paper provides a review of recent advancements and discusses our current knowledge gaps and important emerging research directions.

1. Introduction

1.1. Motivations

The Southwest Pacific Ocean region contains the major oceanic circulation pathway that redistributes waters from the South Pacific subtropical gyre to the equator and high latitudes. The South Equatorial Current (SEC) flows into the Coral Sea, transporting distinct water masses: the salty Upper Thermocline Waters (UTW, $\sigma_\theta \sim$ 24.5 kg m^{-3}) subducted in the dry and windy center of the southeast Pacific gyre (high-salinity patch on Figure 1a; see also *Qu et al.* [2008]; *Hasson et al.* [2013]); the Lower Thermocline Waters (LTW, $\sigma_\theta \sim$ 26.2 kg m^{-3}), in part subducted north east of New Zealand (high-salinity patch on Figure 1b; *Tsubouchi et al.* [2007]; *Qu et al.* [2009]), and the low-salinity Antarctic Intermediate Waters (AAIW, $\sigma_\theta \sim$ 27.2 kg m^{-3}) formed around 50°S [*Qu and Lindstrom*, 2004] and subducted between 170°W and Drake Passage [*Sallee et al.*, 2010; *Hartin et al.*, 2011].

On the poleward pathway, large quantities of heat energy are transported in the East Australian Current (EAC). The main core of the EAC separates from Australia and flows eastward into the Tasman Sea, giving

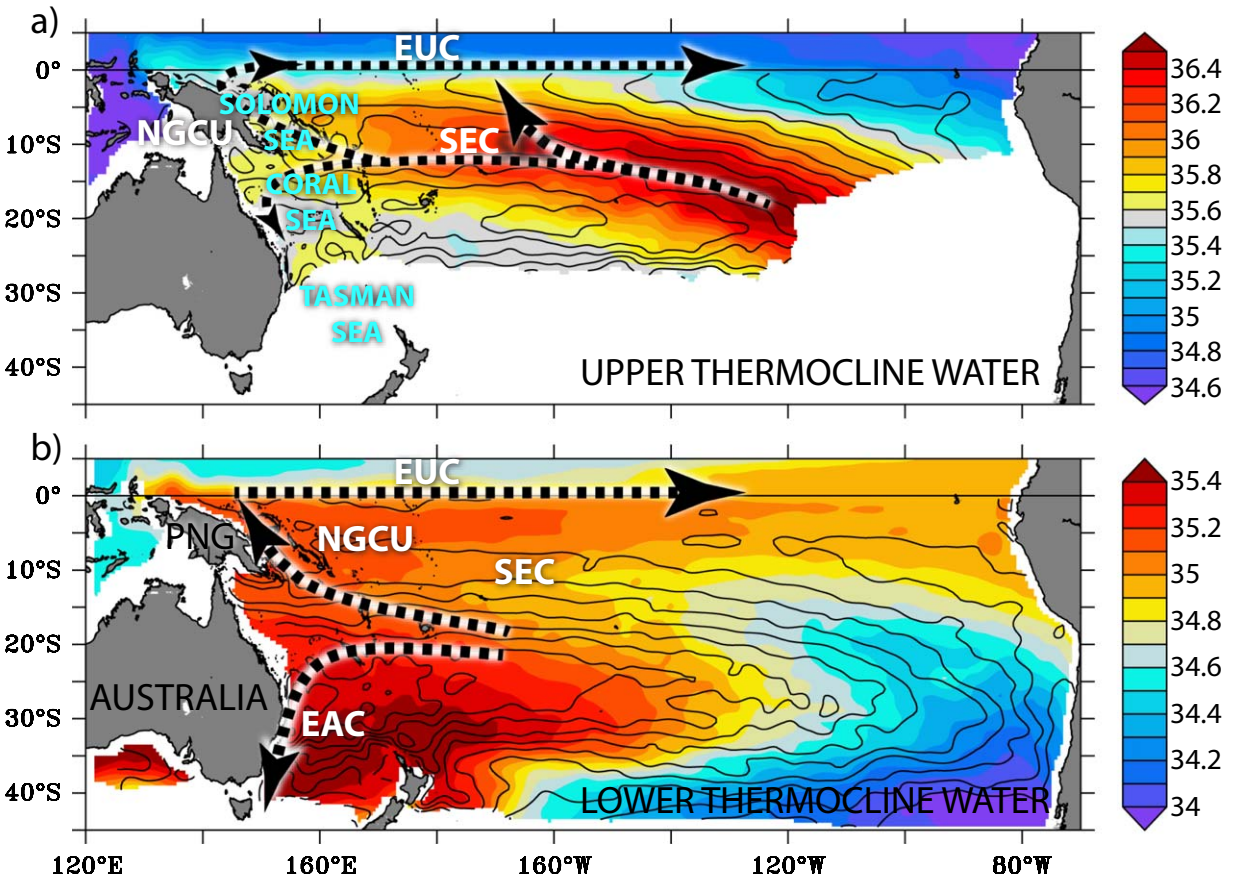

Figure 1. (a) Salinity on isopycnal $\sigma_\theta = 24.5$ kg m^{-3} (color) and geostrophic streamlines (contours) from the CARS climatology [*Ridgway et al.*, 2002]. The dashed arrows represent the approximate pathways of the Upper Thermocline Waters (UTW) b) on $\sigma_\theta = 26.2$ kg m^{-3}; Lower Thermocline Waters (LTW). The two isopycnals correspond, respectively, to the upper and lower part of the Equatorial Undercurrent (EUC). Main currents are indicated: the South Equatorial Current (SEC); New Guinea Coastal Undercurrent (NGCU) as well as the East Australian Current (EAC). Adapted from *Grenier et al.* [2014].

rise to a region of intense eddy activity and air-sea exchanges, with marked influence on climate over Australia and New Zealand [*Sprintall et al.*, 1995]. The remaining EAC continues to flow southward as the *EAC Extension*; where some eventually forms the Tasman Outflow (TO) that connects the South Pacific subtropical gyre with the Indian Ocean, forming a *supergyre* that redistributes water amongst the basins [*Speich et al.*, 2002; *Cai*, 2006; *Ridgway and Dunn*, 2007].

On the equatorward pathway, the Low Latitude Western Boundary Currents (LLWBC) flowing through the Solomon Sea constitute an essential part of the *subtropical cell* circulation [*McCreary and Lu*, 1994]. They contribute to the recharge of the equatorial Warm Pool, and supply the Indonesian Throughflow and the Equatorial Undercurrent (EUC), thereby feeding the downstream surface waters of the cold tongue in the eastern Pacific [*Fine et al.*, 1994]. Documenting the LLWBC transports and properties is important in many ways. On interannual timescales, it has been shown that the LLWBC transport variations partially compensate the interior transport variations [e.g., *Lee and Fukumori*, 2003; *Qu et al.*, 2013]. On decadal timescales, it has been suggested that changes in either the temperature [*Gu and Philander*, 1997] or the amount of water [*Kleeman et al.*, 1999; *McPhaden and Zhang*, 2002] arriving at the equator modify the equatorial thermocline and surface equatorial properties, thus having the capability to modulate the El Niño-Southern Oscillation (ENSO). Temperature and salinity anomalies of O(0.5°C/0.2 psu) can indeed be traced from the southeastern Pacific as they advect toward the west, both in numerical models [*Luo et al.*, 2005; *Nonaka and Sasaki*, 2007; *Qu et al.*, 2013] and Argo float observations [*Kolodziejczyk and Gaillard*, 2012; *Zhang and Qu*, 2014]. Tracking them until they reach the equatorial band is much more difficult, due to the complex LLWBC system and mixing in the Southwest Pacific.

Quantifying the EAC and LLWBC transports and variability in the Coral, Tasman, and Solomon Seas is thus of great importance to climate prediction; documenting hydrological properties and water mass mixing along

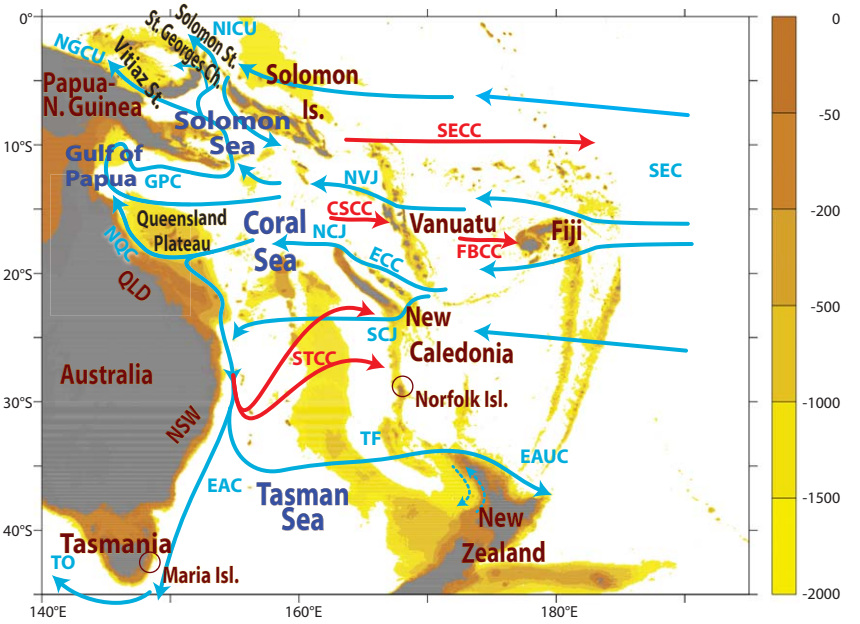

Figure 2. Southwest Pacific topography: only depths shallower than 2000 m are shaded (color scale in meters). The Queensland (QLD) and New South Wales (NSW) coasts are indicated. Blue arrows denote the main currents, integrated 0–1000 m (SEC=South Equatorial Current; NVJ=North Vanuatu Jet; ECC= East Caledonian Current; NCJ=North Caledonian Jet; SCJ=South Caledonian Jet; NQC=North Queensland Current; GPC=Gulf of Papua Current; NGCU=New Guinea Coastal Undercurrent; NICU=New Ireland Coastal Undercurrent; EAC=East Australia Current; TF=Tasman Front; EAUC=East Auckland Current; TO= Tasman Outflow). The red arrows indicate the main surface-trapped counter-currents (STCC=South Pacific Subtropical Counter Current; CSSC=Coral Sea Counter Current; FBCC=Fiji Basin Counter Current; and SECC=South Equatorial Counter Current).

their pathways is also crucial to understand if (and how) anomalies in hydrological properties are transmitted from the subtropical/tropical South Pacific to the equatorial band and to southern Australia. But the oceanic circulation in this region is complex. The bulk of the South Pacific subtropical gyre waters entering the Coral Sea in the broad westward flowing SEC encounter islands, resulting in boundary currents that divide into westward jets at their northern and southern tips, according to the *island rule* dynamics [*Godfrey*, 1989]. These jets include the South Caledonian Jet (SCJ), the North Caledonian Jet (NCJ), and the North Vanuatu Jet (NVJ) (Figure 2). Upon reaching the Australian coast, the NCJ bifurcates and supplies both the EAC and the Gulf of Papua Current (GPC). The GPC enters into the Solomon Sea, becoming the New Guinea Coastal Undercurrent (NGCU) that flows around intricate topography before exiting northward through three narrow passages: the Vitiaz Strait, Solomon Strait, and St. George's channel. To the south, the EAC strengthens as it flows along the coast of Australia. Southward of $\sim 33°$S, it starts to separate into filaments, forming the northwestward South Pacific Subtropical Counter Current (STCC), the eastward Tasman Front (TF, Figure 2), and the EAC extension.

This circulation and its dynamics have been previously identified in numerical simulations [*Webb*, 2000] and low-resolution climatologies [*Qu and Lindstrom*, 2002; *Ridgway and Dunn*, 2003], which motivated enhanced observations to improve their description and understand the connections between currents at different depths, along with the variability. Concurrently, the increased model resolution and bathymetry greatly improved the quality of numerical simulations of the region (section 3). The structure and strength of the Southwest Pacific circulation are related to the southeasterly trade wind structure. Their structure depends on the presence and intensity of the South Pacific Convergence Zone (SPCZ), a region that extends on average from the Solomon Islands to Fiji and southward (see Figure 2) with strong precipitation, wind convergence, and diabatic heating [*Zhang*, 2001]. Modeling the Southwest Pacific circulation is further challenged because our understanding of the SPCZ dynamics is limited, with coupled climate models exhibiting strong biases with the modeled SPCZ extending zonally which is in contrast to the observed SPCZ which slants eastward and turns poleward around the dateline [*Brown et al*., 2011, 2013a].

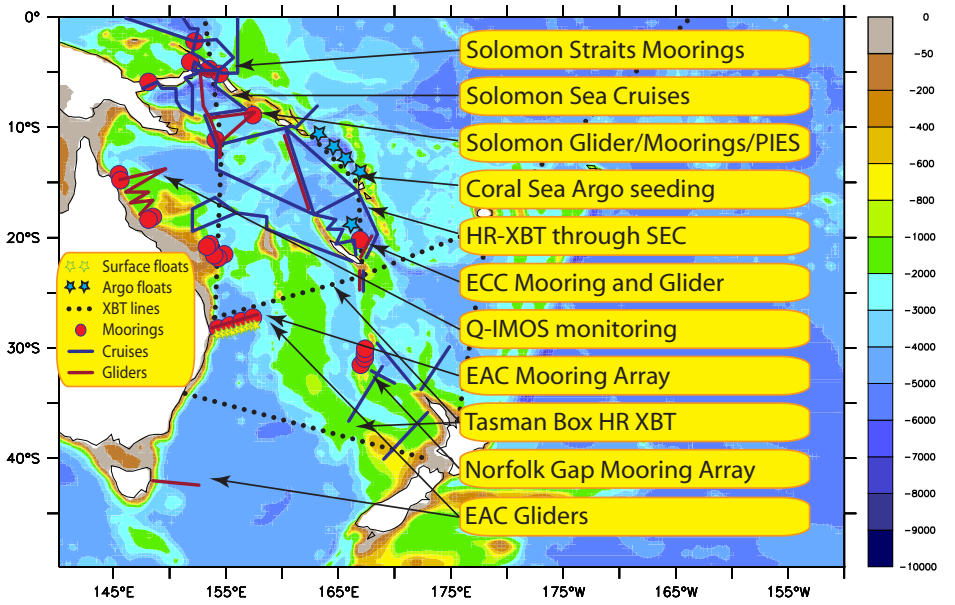

Figure 3. Main elements and regional structure of the SPICE field program, as indicated by the legend: PIES=Pressure Inverted EchoSounder; HR-XBT=High resolution XBTs; Q-IMOS=Integrated Marine Observing System (Queensland node). The background map and colorbar indicates ocean depth.

1.2. SPICE Objectives and Organization

At the outset of the Southwest Pacific Ocean Circulation and Climate Experiment (SPICE) in 2005, relatively few observations were available to diagnose the processes and pathways through the complicated geography of the Southwest Pacific. With most of the region difficult to access, a large temporal variability and strong narrow currents, observations and numerical modeling faced serious challenges. This led scientists from France, Australia, USA, New Zealand, Japan, and Pacific Island countries to develop a coordinated program, including intensive observations and focussed modeling experiments [*Ganachaud et al.*, 2007, 2008a] under the umbrella of the *Variability and Predictability of the Ocean-Atmosphere System* (CLIVAR, http://www.clivar.org) program. SPICE has since been providing a platform to stimulate international collaboration and funding from national programs. The SPICE data are referenced on http://spiceclivar.org.

The main aim of SPICE has been to understand the Southwest Pacific Ocean circulation and its influence on climate, from the Tasman Sea to the equator. This has involved complementary challenges to understand:

1. The circulation, boundary currents, and jets for the different water masses;

2. Transformation and mixing of these waters during their transit;

3. The circulation variability in conjunction with SPCZ dynamics;

4. The impact on equatorial and Tasman Sea water properties; and

5. The key observation metrics whose monitoring is of importance to climate prediction.

These objectives have been addressed through a combination of analysis of historical observations, new observations, and focused modeling efforts. The field programs have measured and monitored the ocean circulation, which have helped validate and improve numerical simulations. In turn, simulations have been used to improve understanding of the dynamics, put observations in context, and provide basic knowledge in unexplored areas.

We have reached a midpoint in SPICE, and we review here the recent progress and new findings. Some work is ongoing and some questions remained unresolved. As research has progressed, new science perspectives have come into view. We start with a description of the overall approach regarding in situ observations (section 2) and numerical modeling (section 3); then review the main scientific advancements along the thermocline pathways in the Coral Sea (subsection 4.1), Tasman Sea (subsection 4.2), and Solomon Sea (section 4.3). We then analyze the oceanic link from the subtropics to the equator and high latitudes

(section 4.4) and discuss SPCZ dynamics (section 4.5). We finish with a summary of the main SPICE advancements and discussion on prospective research (section 5). We provide a list of acronyms in Appendix B.

2. In Situ Observations

The field program was designed to survey the Southwest Pacific inflows, outflows, and Western Boundary Currents (WBCs) quasi-simultaneously in a concerted attempt to close the regional mass, heat, and freshwater budgets. An important purpose was also to test ocean transport monitoring technologies (Figure 3). High-resolution hydrographic surveys provided temperature, salinity, and dissolved oxygen down to at least 2000 m; nutrient and geochemical data were collected on several cruises, in coordination with the international program GEOTRACES (http://www.geotraces.org).

Some glider deployments first served to demonstrate the application of recent technology with lines in two coastal jets near New Caledonia (subsection 4.1); across the western boundary currents off Queensland and New South Wales (subsection 4.1 and 4.2); and in the Solomon Sea (section 4.3). The SEC transport into the Coral Sea is currently monitored through High Resolution eXpendable BathyThermograph (HR-XBT) transects (see below), a mooring and colocated glider measurements. The Australian Integrated Marine Observing System (IMOS) includes specific assessment of the impacts of the boundary currents on the Great Barrier Reef (GBR, that extends about 3000 km along the WBCs) and Tasman Sea. Remote sensing, mooring arrays, and glider surveys have been operating there since 2007. Off the GBR, four pairs of moorings are distributed on the continental slope and on the outer shelf, between 23°S and 14°S to measure the GPC and the low-latitude part of the EAC, as well as exchanges across the shelf.

To the north, gliders from Scripps Institution of Oceanography/National Oceanic and Atmospheric Administration have monitored the transport across the south entrance of the Solomon Sea, with four to eight crossings annually since 2007 (subsection 4.3). Those are now supplemented by Pressure Inverted EchoSounders (PIES) to provide horizontal integrals of mass and heat transport at high temporal resolution through a combination of the two data sets. Moorings were deployed in the Solomon Straits and off New Ireland (subsection 5.2). These coordinated measurements are expected to help document the transport size, variability, and partition amongst the Solomon Straits.

Two current meter arrays were deployed in the Tasman Sea: one across the EAC, against the coast of Australia near 27°S, and another one in the deep pathways south of Norfolk Island to measure the TF flow (subsection 4.2). HR-XBT sections provide high-resolution temperature surveys of the upper water column and associated oceanic transports. Initiated in 1991 across the "Tasman box" (Fiji-Australia-New Zealand, Figure 3), those have continued in conjunction with new meridional sections east [*Maes et al*., 2011] and west [*Goni et al*., 2010] of the Coral Sea. On a regular basis, surface drifters were also released during cruises or HR-XBT lines, with an enhanced focus across the EAC [*Brassington et al*., 2011].

Argo floats seeded in the Southwest Pacific during SPICE increased the number of temperature and salinity profiles from ~700 per year in 2005 to ~2600 per year in 2013. Argo floats are now released on a regular basis in the Southwest Pacific, with a major deployment taking place in 2012 (75 floats, mostly equipped with Iridium transmission to avoid long surface times and associated stranding risk).

3. Modeling Ocean Dynamics

A variety of global and regional ocean models, from coarse resolution up to eddy-resolving spatial scales ($\leq$10 km), have been used to explore mesoscale activity [e.g., *Everett et al*., 2012], multidecadal climate trends [e.g., *Hill et al*., 2011] and link coastal impacts to regional and global phenomena such as ENSO [e.g., *Melet et al*., 2013], global warming [e.g., *Sen Gupta et al*., 2012], and the Interdecadal Pacific Oscillation [e.g., *McGregor et al*., 2009a] (section 4). Simple to intermediate complexity ocean models have also been used to understand the dynamic mechanisms that underpin the seasonal to decadal upper ocean variability down to the thermocline [e.g., *Kessler and Gourdeau*, 2007; *McGregor et al*., 2007, 2008, 2009b; *Holbrook et al*., 2011]. Furthermore, there is an increasing synergy between climate modeling and operational oceanography efforts such as those pursued by forecasting initiatives like MERCATOR Ocean (1/12°, http://www.mercator-ocean.fr) and BLUElink [1/10°, *Schiller et al*., 2009a; *Oke et al*., 2012]. Combining these models with observations has enabled the exploration and analysis of:

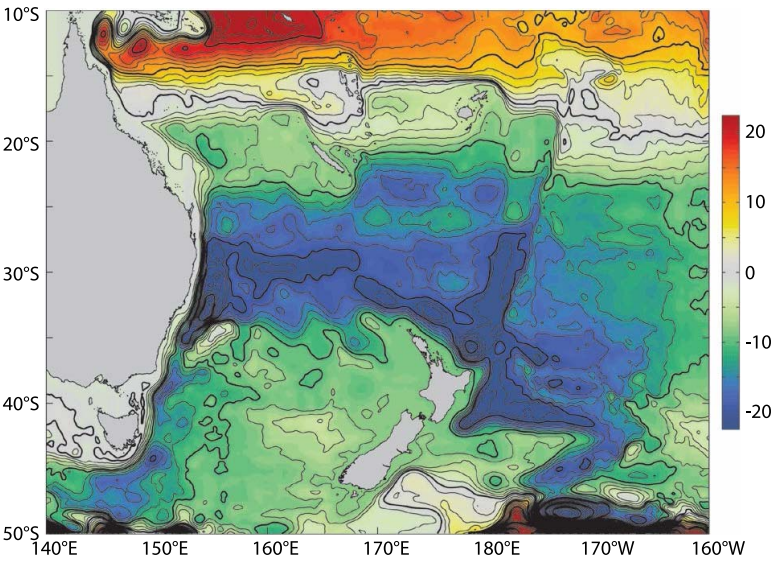

Figure 4. OFAM3 model full-depth transport streamfunction [*Oke et al.*, 2013]. Contour interval is 1 Sv (1 Sv = $10^6 m^3 s^{-1}$).

1. Jet-like structures in the SPICE area (subsection 4.1; dynamics of the NCJ and NVJ) [*Couvelard et al.*, 2008];
2. Eddy dynamics in boundary currents such as the EAC, GPC, and in the Solomon Sea (subsections 4.2 and 4.3) [*Brassington et al.*, 2011; *Oke and Griffin*, 2011; *Oke et al.*, 2013; *Gourdeau et al.*, 2014];
3. Subduction zones, water circulation, and pathways (subsection 4.4) [e.g., *Grenier et al.*, 2011, 2014; *Qu et al.*, 2013];
4. Shelf-scale, islands, and upwelling processes (subsection 5.4.3; Australia coastal currents; New Caledonia upwelling) [*Schiller et al.*, 2008; *Marchesiello et al.*, 2010]; and
5. Dynamical drivers of sea surface temperature (SST) anomalies in the Coral Sea and associated coral bleaching events (subsection 5.4.3) [*Schiller et al.*, 2009b].

Figure 4 illustrates the main features of the large-scale circulation in the SPICE domain as simulated with the recent near-global version of the Bluelink OFAM3 model [*Oke et al.*, 2013]. In the eddy-resolving ocean ReANalysis (BRAN, 1/10° resolution), the model captures the main gyre cells and circulation features, including EAC transport; connection with topography; jets; the SEC bifurcation; the TF; quasi-stationary eddies north of New Zealand and the EAC Extension towards Tasmania and its associated TO.

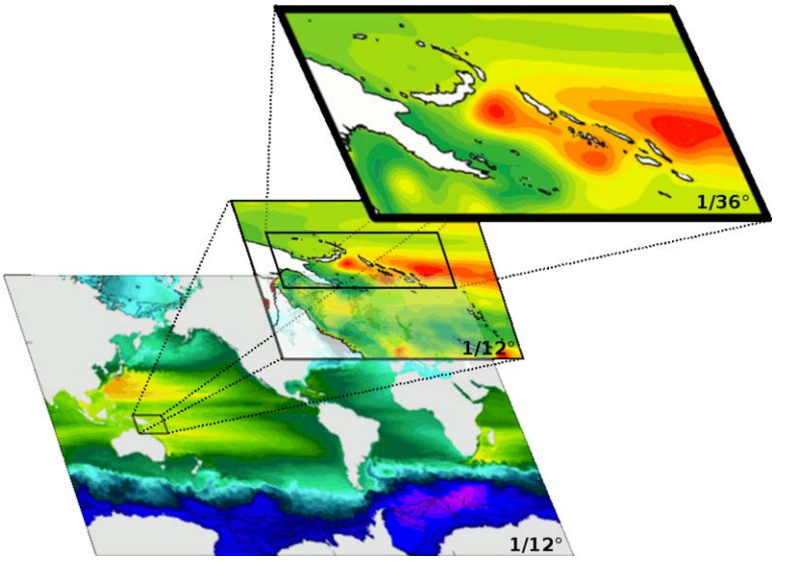

Figure 5. Numerical model nesting schematics over the Solomon Sea. The high resolution 1/36° regional model is embedded within a 1/12° basin model of the South West Pacific through a two-way interactive connection, whereas the 1/12° regional model is itself embedded in the 1/12° global configuration from the DRAKKAR project (http://www.ifremer.fr/lpo/drakkar). From *Djath et al.* [2014a].

An operational model has been developed specifically on the GBR, Bluelink-OceanMaps, to understand coastal and riverine impacts on the GBR. This system is also used to understand Coral Sea influences on the GBR, and utilizes IMOS observations for validation.

A large modeling effort was devoted to the Solomon Sea, as the complex bathymetry with numerous straits and islands is particularly challenging (subsection 4.3), and high resolution is required to resolve the narrow straits that connect with the equator. The Adaptive

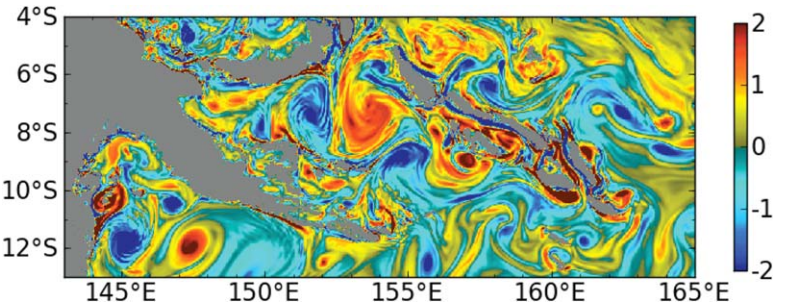

Figure 6. Potential vorticity at 20 m depth on 31 March 1995 from the 1/36° resolution NEMO Solomon Sea model simulations (full PV; unit is 10^{-7} kg m^{-4} s^{-1}).

Grid Refinement (AGRIF) nesting system (Figure 5) has been implemented to refine the model resolution to 1/12° in a 1/4° global model [*Melet et al*., 2010a], providing a first description of the circulation, variability, and water mass transformations (subsection 4.3). An original approach based on both one-way (boundary forced) and two-way (fully interactive) configurations enabled development of a high-resolution model that interactively connects with the circulation of the Southwest Pacific region (Figure 5). In parallel, an exploratory data assimilation analysis allowed evaluation of the potential impact of glider observations on the simulation of the Solomon Sea circulation, including tidal mixing parameterization, and proposed guidance to deployment strategies [*Melet et al*., 2012].

Modeling has also been used to explore the role that the Solomon Sea could play in the water mass transformation and the feedback to the EUC, including at ENSO timescales (subsection 4.4) [*Grenier et al*., 2011; *Melet et al*., 2011, 2013]. These experiments suggest that diapycnal mixing sustained by internal tide breaking is significant in the Solomon Sea and needs to be parameterized following, e.g., *Koch-Larrouy et al*. [2007].

Recently, very high-resolution experiments (1/36°) targeted mesoscale and submesoscale variability in the Solomon Sea. Two distinct models have been used: one with the terrain-following sigma-coordinate ROMS model [*Hristova et al*., 2014] and the other one with a z-coordinate model NEMO [Figure 6; *Djath et al*., 2014a, 2014b]. Both models better represented the observed circulation of the Solomon Sea (subsection 4.3) [*Djath et al*., 2014b]. This configuration allowed a full resolution of mesoscale processes ("eddy-resolving models") and a marginal resolution of submesoscales ("sub-mesoscale permitting models"), that led to new fields of exploration (subsection 5.4.1).

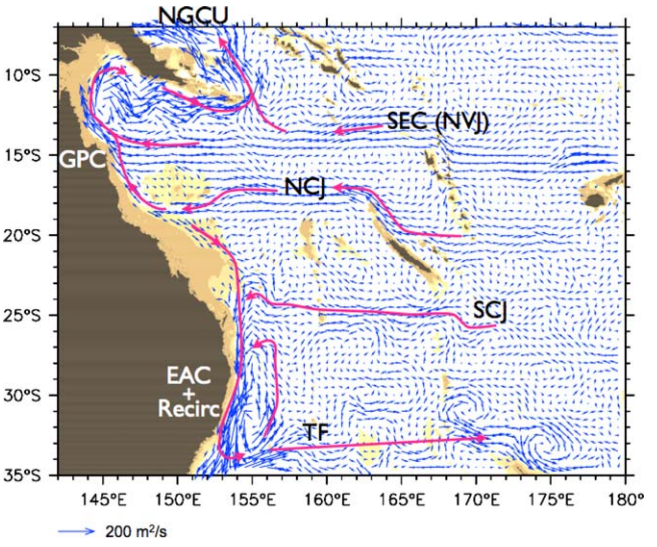

Figure 7. 0–1000 m transports estimated from the relative geostrophic velocity from CARS climatology [*Ridgway et al*., 2002] combined with mapped average absolute velocity at 1000 m from Argo float drift. The main currents are indicated as in Figure 2. From *Kessler and Cravatte* [2013a].

4. Scientific Advancements

4.1. Coral Sea

SPICE observations and models have confirmed and refined previous Coral Sea circulation schematics (Figure 7), quantified transports, and revealed the vertical structures: a broad and shallow NVJ transports ~20 Sv (Figure 8a) and a narrow and deep NCJ extending to at least 1500 m (Figure 8b) transports ~12 Sv [*Kessler and Gourdeau*, 2007; *Gourdeau et al*., 2008; *Ganachaud et al*., 2008b]. Observations revealed two unexpected features: (1) the deep extent of the NCJ and (2) the conspicuous surface signature of the jets (missing from early descriptions, e.g., *Qu and Lindstrom* [2002] but revealed in recent drifter

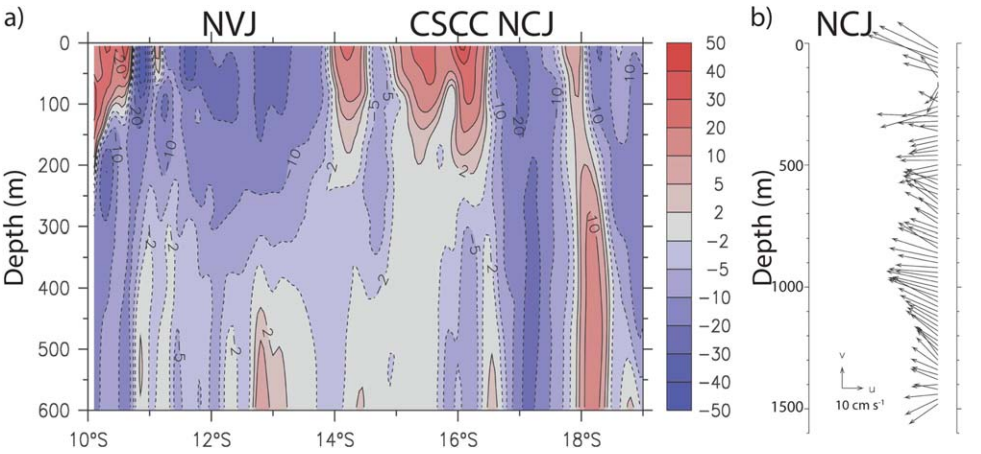

Figure 8. (a) Absolute cross-track geostrophic velocity (cm s^{-1}) determined by a glider crossing from the Solomon Islands to New Caledonia (red indicates eastward and blue westward). (b) Velocity measured Acoustic Doppler Current Profilers (ADCP) in the center of the NCJ at 17.77°S. Eastward currents plotted to right, northward up (see scale key). The NVJ, CSCC, and SCJ are indicated. Adapted from *Gourdeau et al.* [2008].

observations [*Choukroun et al.*, 2010]). Limited observations suggest the presence, at least episodically, of a subsurface jet south of New Caledonia (the SCJ). While the existence of these jets was remarkably well predicted by the linear *Island Rule* [*Qiu et al.*, 2009], topographic effects and nonlinearities are needed to explain the predominance of the northern jets compared to the southern jets [*Couvelard et al.*, 2008]. In the lee of Vanuatu Islands and just south of the NVJ, an eastward current was found and named the Coral Sea Counter Current [CSCC, *Qiu et al.*, 2009, see Figure 8a]. The same authors found an eastward countercurrent to the west of Fiji, the Fiji Basin Countercurrent (FBCC, Figure 2). The existence of these surface countercurrents have been explained using Sverdrup balance and localized wind stress curl dipoles generated by the island mountains [*Qiu et al.*, 2009], although *Couvelard et al.* [2008] argued that they are due to nonlinear advection.

An important outcome of SPICE was to ascertain that the NQC, the Great Barrier Reef Undercurrent (GBRUC, beneath the NQC) [*Church and Boland*, 1983] and the Hiri Current, south of PNG [*Burrage*, 1993] were all part of a continuous WBC that flows around the Gulf of Papua and propose a unified name, the GPC [*SPICE Community*, 2012].

The connection between these different Coral Sea currents are depth dependent and can be inferred from dissolved oxygen and salinity. *Gasparin et al.* [2014] propose a formal assessment of water mass contributions for different parts of the Coral Sea that confirms and quantifies inferences from salinity and oxygen. The shallow NVJ is supplied by SEC waters flowing north of Fiji, or essentially UTW. Part of it turns directly into the Solomon Sea in midbasin (the *direct* NVJ pathway, Figure 7); this pathway, whose dynamics are not well understood, is the shortest WBC pathway to the equator (subsection 4.3). The other part continues west where it bifurcates and contributes to the northward GPC and southward EAC [*Kessler and Cravatte*, 2013a].

On encountering New Caledonia, the SEC forms the East Caledonian Current (ECC), which then separates as the NCJ [*Gasparin et al.*, 2011]. The ECC/NCJ mainly advect oxygenated LTW from the part of the SEC south of Fiji Island and fresh AAIW below that [*Maes et al.*, 2007; *Gasparin et al.*, 2011].

The bifurcation at the Australian continent is vertically tilted: most of the NVJ transport turns north, except for a tongue of shallow waters above σ=25 kg m^{-3} that turns south to begin the EAC at 15°S. Waters from the NCJ, deeper than σ=26 kg m^{-3}, arriving at the coast turn north to feed the GPC, while waters lighter than σ=26 kg m^{-3} turn south to feed the EAC [*Kessler and Cravatte*, 2013a]. The bifurcation thus occurs in both jets, with a surface water bifurcation in the NVJ and a deep water bifurcation in the NCJ. The structure of the bifurcation is complicated by the large Queensland Plateau (150°E, 17°S) [*Choukroun et al.*, 2010].

The EAC and GPC also impact the GBR. Long-term surveys show the GBR has lost half its coral cover in the last 27 years because of storm damage (~ 50%), crown of thorns starfish (~ 40%), and bleaching (~ 10%) [*De'ath et al.*, 2012]. IMOS GBR mooring array, glider surveys operating since 2007 (section 2), and an

operational model (section 3) have monitored shelf exchanges. Significant GPC/EAC intrusions and stratification occur during spring to late summer, with consequences for the ecosystem that include coral bleaching due to warming events [*Berkelmans et al*., 2010] and potential outbreaks of crown-of-thorns starfish due to increased nutrients from offshore upwelling.

The SEC, the jets, and the WBCs respond to large-scale forcing, either locally under direct wind influence, or remotely through ocean wave propagation, depending upon latitude and timescales. At interannual timescales, an El Niño event generally enhances the SEC transport entering the Coral Sea [*Kessler and Cravatte*, 2013b] particularly in the NVJ, with a simultaneous increase in the transport entering into the Solomon Sea (see subsection 4.3). Cold temperature anomalies then propagate westward and bifurcate to the north and south a few months later [*Holbrook et al*., 2005a, 2005b]. The interannual variability of the other WBCs and jets is less well described or understood and should be explored in future studies.

At seasonal timescales, Rossby waves play an important role in setting the timing for thermocline depth fluctuations in the Coral Sea [*Holbrook and Bindoff*, 1999]. The subtropical gyre spins up during austral spring, producing larger transports at its northern end, near 10°S, with a maximum in November [*Kessler and Gourdeau*, 2007]. This results in increased equatorward transport into the Solomon Sea and poleward transport anomalies along the entire East Australian coast about 1 month later, shifting the NCJ bifurcation latitude northward. At intraseasonnal timescales, the Coral Sea jets and countercurrents result in high variability from dynamical instabilities [*Qiu et al*., 2009]. At weekly timescales, strong anomalous temperatures events can also be generated by both local and remote influences [e.g., heat waves on the GBR, *Schiller et al*., 2009b]. The resulting top-to-bottom transport entering the Coral Sea is close to 25–30 Sv, with $\pm$6 Sv seasonal variations, and maximum transports in the second half of the year [*Kessler and Gourdeau*, 2007]. Interannual variations are of order $\pm$10 Sv, with maximum transports during El Niño phases [*Kessler and Cravatte*, 2013b]. In addition, synoptic eddies can create substantial changes over a few weeks [*Kessler and Cravatte*, 2013b, Table 1].

4.2. Tasman Sea

The EAC originates at approximately 15°S in the surface NVJ bifurcation (Figure 1) [*Church and Boland*, 1983]. South of 19°S, the total volume transport of the EAC increases due to the arrival of the deeper NCJ waters and by the SCJ ($\sim$23°S) [*Kessler and Cravatte*, 2013a]. Between 18°S and 35°S, the southward transport generally increases, ranging from 25 to 36 Sv near 28°S, the latter value including waters that are recirculated immediately east of the EAC [*Ridgway and Godfrey*, 1997]. The bulk of the EAC separates from Australia between 32°S and 34°S forming the broad meandering eastward TF [*Ridgway and Dunn*, 2003] and associated region of large mesoscale variability [e.g., *Bowen et al*., 2005].

The TF extends across the Tasman Sea with part of the flow continuing into the Pacific and a portion reattaching to the northern end of New Zealand as the EAUC (Figure 2) and a sequence of semi-permanent eddies along the east coast of the New Zealand Islands [e.g., *Tilburg et al*., 2001]. The EAUC finally converges with the subtropical front and both currents turn eastward in a confluence region [Figure 4; *Fernandez et al*., 2014]. The TF transport through the Norfolk gaps (on Figure 3) was estimated at 6 $\pm$ 4 Sv in the upper 800 m, overlying 2 $\pm$ 2 Sv of westward flowing AAIW [*Sutton and Bowen*, 2014]. Limited observations in the 1950s also suggested a southward flow of subtropical water from the TF along the northwest coast of New Zealand, which had been named the West Auckland Current. However, a current meter array and repeat hydrographic sections show no evidence of such a current, only weak southward flow offshore of the 1000 m isobaths and northward flow inshore [*Sutton and Bowen*, 2011].

Much of our understanding of the EAC system has been developed from in situ observations collected over many decades. However, these data are irregularly distributed in both space and time and are not generally suitable for resolving the large interannnual to decadal variability [*Ridgway et al*., 2002]. Since 1992, altimetric data have greatly improved the data coverage and have been combined with the repeated, eddy-resolving *Tasman Box* HR-XBT (Figure 3) to estimate EAC transport time series between Australia and New Zealand [*Ridgway et al*., 2008]. Both the TF separation latitude and the EAC transport vary seasonally—the EAC is strongest in summer (36 Sv) and weakest in winter (27 Sv) at 28°S [*Ridgway and Godfrey*, 1997]. The EAC varies on interannual timescales, but only a small fraction of the variance is correlated with ENSO [*Ridgway and Dunn*, 2007].

Conversely, the EAC has strong decadal signals, as measured in temperature, salinity, and sea level [*Sutton et al., 2005; Ridgway and Dunn*, 2007; *Ridgway et al*., 2008; *Holbrook et al*., 2011]. Over the past 12 years, the

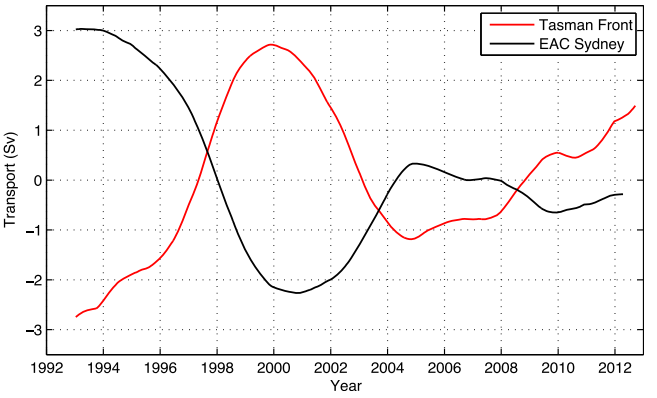

Figure 9. The EAC Extension transport variations observed off Sydney (blue curve) and the Tasman Front/East Auckland Current (red curve) obtained from a combined XBT and altimeter data set [*Ridgway et al.*, 2008]. Each time series has been low-pass filtered with a 5 year cut off.

South Pacific Gyre was observed to accelerate, in concert with an increased EAC Extension [*Roemmich et al.*, 2007; *Ridgway*, 2007] and intensification of the wind stress curl east of New Zealand. A 50 year ocean reanalysis suggests the occurrence of a *gating* effect between the EAC Extension and the TF on decadal timescales: increased wind stress curl over the South Pacific causes larger transport in the EAC Extension (and western boundary currents off New Zealand at the same latitudes) and smaller transport in the TF; decreased wind stress curl has the opposite effect [Figure 9; *Hill et al.*, 2011]. These variations are consistent with Island Rule dynamics [*Hill et al.*, 2011; *Fernandez et al.*, 2014; *Oliver and Holbrook*, 2014a] along with changes in the wind stress curl attributed to the Southern Annular Mode [*Cai*, 2006; *Roemmich et al.*, 2007]. Alternatively, observational and modeling studies attribute the changes to decadal ENSO variations in the subtropics and propagation through ocean waves [*Holbrook et al.*, 2005a, 2005b; *Sasaki et al.*, 2008; *Holbrook et al.*, 2011]. These divergent interpretations suggest that the physical connections between the wind stress curl and the changes of the boundary current system still need investigation.

These decadal and longer term variations have local consequences: for instance, during El Niño years, winter SST around New Zealand tends to be cooler [*Sutton and Roemmich*, 2001], with increased Subtropical Mode

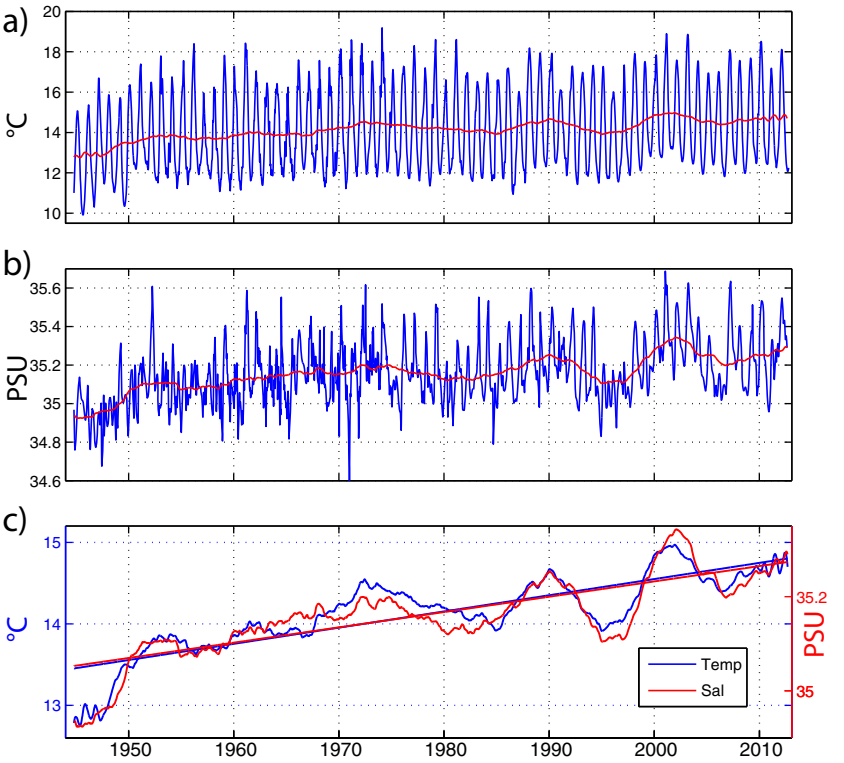

Figure 10. The (a) temperature and (b) salinity time series from the Maria Island station [*Ridgway*, 2007]. In (c) each of the series has been low-pass filtered and normalized with their standard deviations. The long-term trend is also shown.

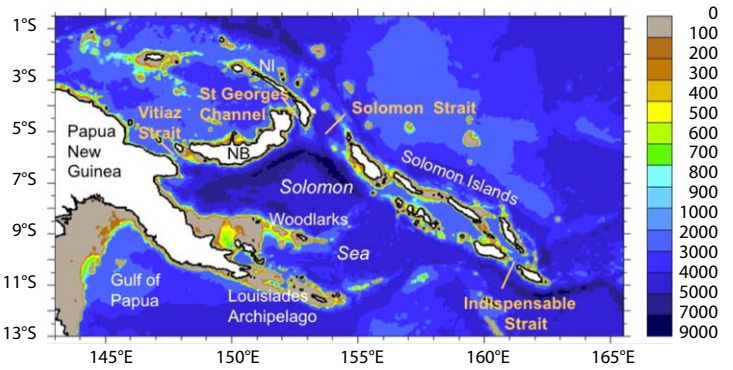

Figure 11. Solomon Sea topography. The bottom depth is indicated by the shading (color scale in meters). The large Islands are noted NI (New Ireland) and NB (New Britain).

Water (STMW) production, which feeds the LTW (section 1) [*Sprintall et al*., 1995; *Holbrook and Maharaj*, 2008]. STMW production may be further enhanced or reduced by the contribution from the dynamical modulation of the EAC/TF by incoming Rossby waves [*Tsubouchi et al*., 2007; *Holbrook et al*., 2011].

Off Tasmania's east coast, the long-term record from Maria Island (Figure 2) shows that the southward penetration of the EAC Extension has increased by approximately 350 km over the past 60 years, and the region has become both warmer $\sim +1°$C ($\sim +2.3°$C/century) and saltier $\sim +0.3$ psu at the sea surface (Figure 10) [*Ridgway*, 2007]. An earlier analysis over the 1955–1988 period noted a $\sim +1.5°$C/century vertically integrated warming over the upper 100 m in the same area [*Holbrook and Bindoff*, 1997]. The EAC Extension is projected to further intensify during the 21st century at the expense of the TF, in response to increases in the wind stress curl south of the EAC separation latitude [*Oliver and Holbrook*, 2014a].

4.3. Solomon Sea

The Solomon Sea is the main route toward the equator and contains intense flows and intricate topography (Figure 11). Before SPICE, the circulation was almost undocumented: it was based on sparse in situ measurements that consisted of scattered Acoustic Doppler Current Profiler (ADCP) and XBT data collected during ship transits. Three SPICE cruises were dedicated to the area, along with gliders and repeated deployments of Argo floats, to provide an unprecedented observational database. The net inflow from the Coral Sea was estimated to be 30 Sv over 0–2000 m from a 2007 hydrographic cruise [Figure 12b; *Gasparin et al*., 2012]. The mean transport from 2007 to 2011 was estimated from repeated glider measurements at 15 Sv in the upper 0–700 m, although the variability was as strong as the mean transport [see below, *Davis et al*., 2012]. An analysis from Argo floats suggested a similar 2004–2011 mean transport at $\sim$19 Sv over 0–1000 m [*Zilberman et al*., 2013].

A model system with a 1/12° resolution within the Solomon Sea, interactively nested in a 1/4° resolution domain (section 3), enabled a first description of the mean and seasonal thermocline circulation [Figure 12a; *Melet et al*., 2010a]. These results were confirmed or corrected using a shipboard ADCP velocity climatology [Figure 12b; *Cravatte et al*., 2011]. At the thermocline level, the NGCU is fed by both the GPC, with a core near $\sigma_\theta = 26.5$ kg m^{-3} (around 400 m), and more directly by the shallower NVJ (Figures 12a and 12b). In the Solomon Sea, the time-mean, equatorward flowing NGCU splits at the Woodlark Archipelago (Figure 12b), joins again, then bifurcates at the southern coast of New Britain. A westward branch flows through Vitiaz Strait, and an eastward branch forms the New Britain Coastal Undercurrent (NBCU), which exits St Georges Channel and Solomon Strait to subsequently form the St Georges Undercurrent (SGU) and the New Ireland Coastal Undercurrent (NICU), respectively [Figures 12a and 12b; *Melet et al*., 2010a; *Cravatte et al*., 2011]. This NGCU partition leads to different connecting pathways from the Solomon Sea to the equatorial Pacific (section 4.4); its variability is partly related to a restriction of the flow through Vitiaz St that deviates additional transport towards Solomon Strait [*Melet et al*., 2010a].

Thermocline waters of the SEC also enter the Solomon Sea through the eastern part of Solomon Strait (5°S), and through Indispensable Strait (Figure 11). The *Melet et al*. [2010a] numerical simulation suggested that this southward Solomon Strait inflow mainly originated from a secondary western boundary current (0–300 m) east of the Solomon Islands chain which the authors labeled the *Solomon Island Coastal Undercurrent (SICU)*. In contrast, the recent high-resolution simulations of *Hristova et al*. [2014] and *Djath et al*. [2014b] both show varying flow direction with depth east of the Solomon Island chain, with very strong seasonal variability, as also observed in surface drifters [*Hristova and Kessler*, 2012]. The connection of those currents with the rest of the boundary current

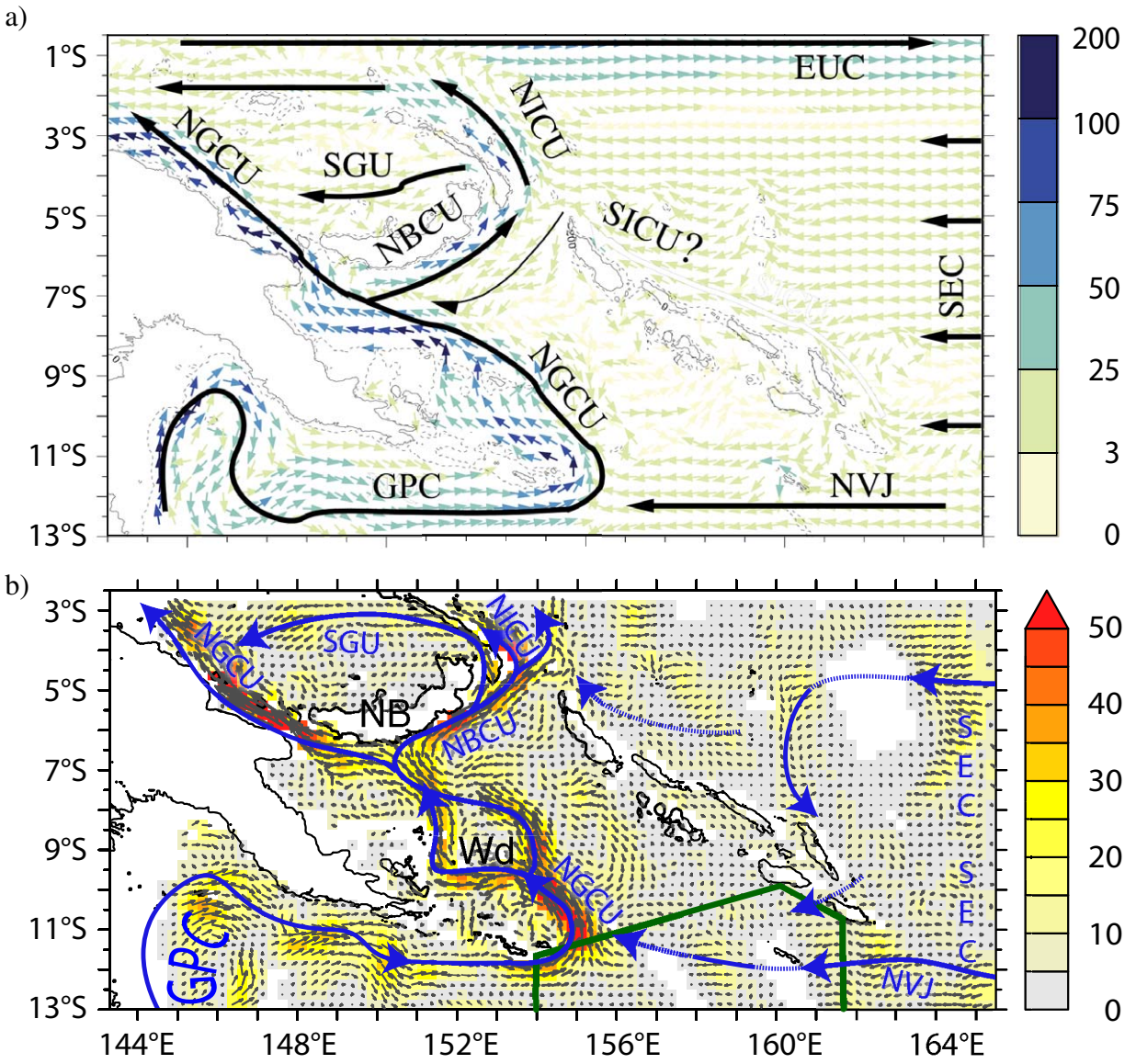

Figure 12. Mean circulation in the Solomon Sea thermocline. (a) From the 1986–2004 mean of a 1/12° simulation, and vertically integrated from the isopycnal surfaces $\sigma_\theta = 24.0$ to 26.5 kg m^{-3} [adapted from *Melet et al.*, 2010a]. (b) From a climatology of shipboard-ADCP data, averaged over the 100–300 m layer adapted from *Cravatte et al.* [2011]. In (b), the green straight lines locate the 2007 oceanographic cruise track (see text) New Britain (NB) and the Woodlark Archipelago (Wd) are indicated, as well as the main currents as on Figure 2, as well as St George Undercurrent (SGU); New Britain Coastal Undercurrent (NBCU); and an hypothetical Solomon Island Coastal Undercurrent (SICU; see text).

system is also seasonally variable. We prefer to avoid attributing any current name at this stage as the models are in an early phase of analysis and there are only two point-wise observations from cruises.

Near 10°S, the southwestward inflow of SEC waters from Indispensable Strait is revealed by its contrasted salinity and dissolved oxygen [*Gasparin et al.*, 2012]. However, its transport is still not known accurately, and is probably highly variable (the high-resolution simulation of *Djath et al.*, [2014a], suggests a 1 ± 3 Sv inflow with a well-marked annual cycle). The circulation in the surface and thermocline layers differs predominantly in the eastern Solomon Sea. Most striking is the Solomon Strait circulation, with a southward flow in the upper ~100 m above the (northward) NICU [*Cravatte et al.*, 2011].

Altimetry revealed that the highest sea level variability in the tropical South Pacific was found east and west of the Solomon Islands in response to both basin-scale variations [*Melet et al.*, 2010b] and local mesoscale eddies [*Gourdeau et al.*, 2014; *Hristova et al.*, 2014]. In addition, the mesoscale eddy activity is modulated by the circulation in the Solomon Sea at seasonal and interannual timescales

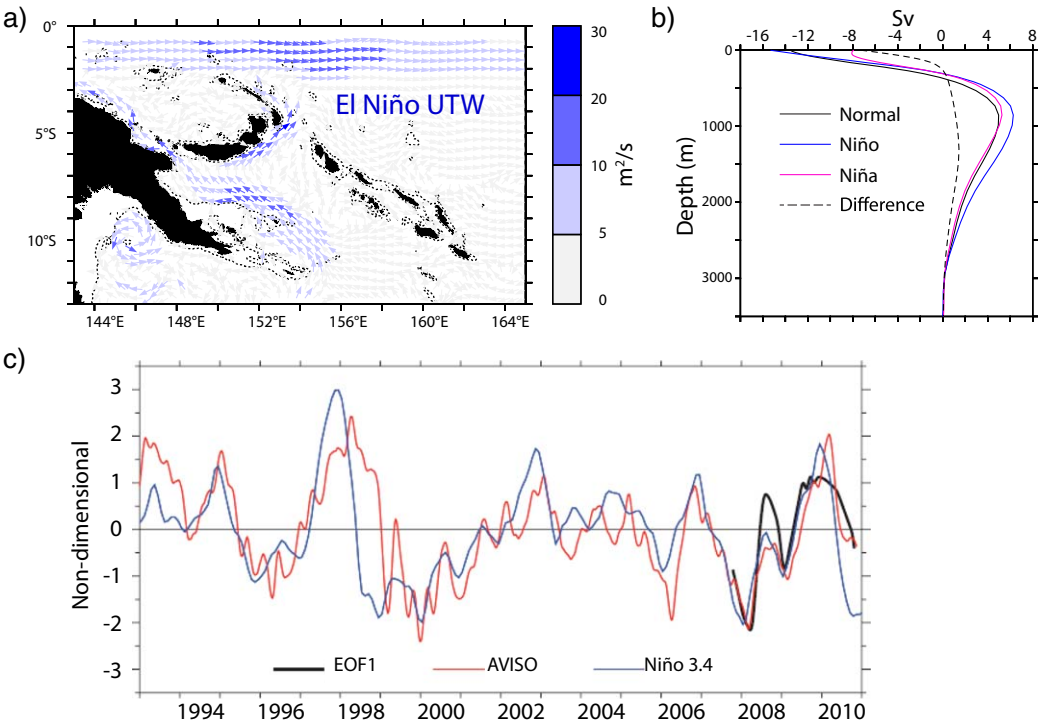

Figure 13. Interannual variability of the Solomon Sea circulation. (a) Circulation anomalies vertically integrated in the upper thermocline ($23.3<\sigma_0<25.7$ kg.m^{-3}) during El Niño, from composites in the 1/12° simulation. (b) Depth cumulated transport (Sv from 3500 m) during the winter (November–February) at the Solomon Sea southern entrance (9.8°S) for the mean state (black line), El Niño state (blue line), and La Niña state (magenta line). The difference between El Niño and La Niña is plotted as a black-dashed line [see *Melet et al.*, 2013]. (c) Time series of the smoothed Solomon Sea equatorward geostrophic surface transport per unit depth from Aviso altimetric data (red line), and the equatorward transport per depth by the dominant EOF of upper layer transport computed from glider data (black line). The Nino 3.4 sea surface temperature anomalies are also shown (blue line) to indicate variability associated with ENSO. [adapted from *Davis et al.*, 2012].

[*Gourdeau et al.*, 2014]. The seasonal cycle has been observed, with a strengthening of the WBCs in austral winter (JJA) [*Cravatte et al.*, 2011; *Hristova and Kessler*, 2012] and results from the combination of equatorial waves, different regimes of Rossby waves east and south of the Solomon Sea, and the local wind influence [*Melet et al.*, 2010a]. On interannual timescales, repeated glider transects [*Davis et al.*, 2012] and the *Melet et al.* [2013] numerical simulation revealed large transport variations up to ~100% of the mean transport occurring mainly away from the boundary current, in the upper 250 m (Figures 13a and 13b). The LLWBCs counterbalance meridional transport anomalies over the rest of the South Pacific and vary in phase with ENSO as is also observed in altimetric and Argo data [Figure 13c; *Melet et al.*, 2010b; *Zilberman et al.*, 2013]. In the model, the NGCU transport increases during an El Niño event and, due to the transport restriction through Vitiaz Strait, positive transport anomalies are mostly transmitted to Solomon Strait. (Figure 13a).

Zilberman et al. [2013] estimated the heat transport through the meridional overturning circulation (an equatorward inflow of 30 Sv above 1000 m in balance with southward outflow in the surface layer) to be between 0.4 and 0.6 $\times$ 10^{15} W (PW) across the Pacific, including the NGCU contribution. This heat transport also exhibits substantial interannual variations ($\pm$0.3 PW) across the basin, partly associated with the large NGCU transport variations [*Melet et al.*, 2013].

4.4. Link to the Equator and High Latitudes

4.4.1. Oceanic Pathways to the Equator, and Their Variability

Early numerical simulations suggested that about 2/3 of the EUC originated from the South Pacific [e.g., *Blanke and Raynaud*, 1997]. The refined model analysis of *Grenier et al.* [2011] diagnosed that about 70% of EUC water at 156°E comes from the Solomon Sea or just east of the Solomon Islands. As described in subsections 4.1–4.3, the circulation pathways are depth and time-dependent, as is the partition of the water transports in the different equatorward branches (spaghetti arrows on Figure 14a and Appendix A). Because

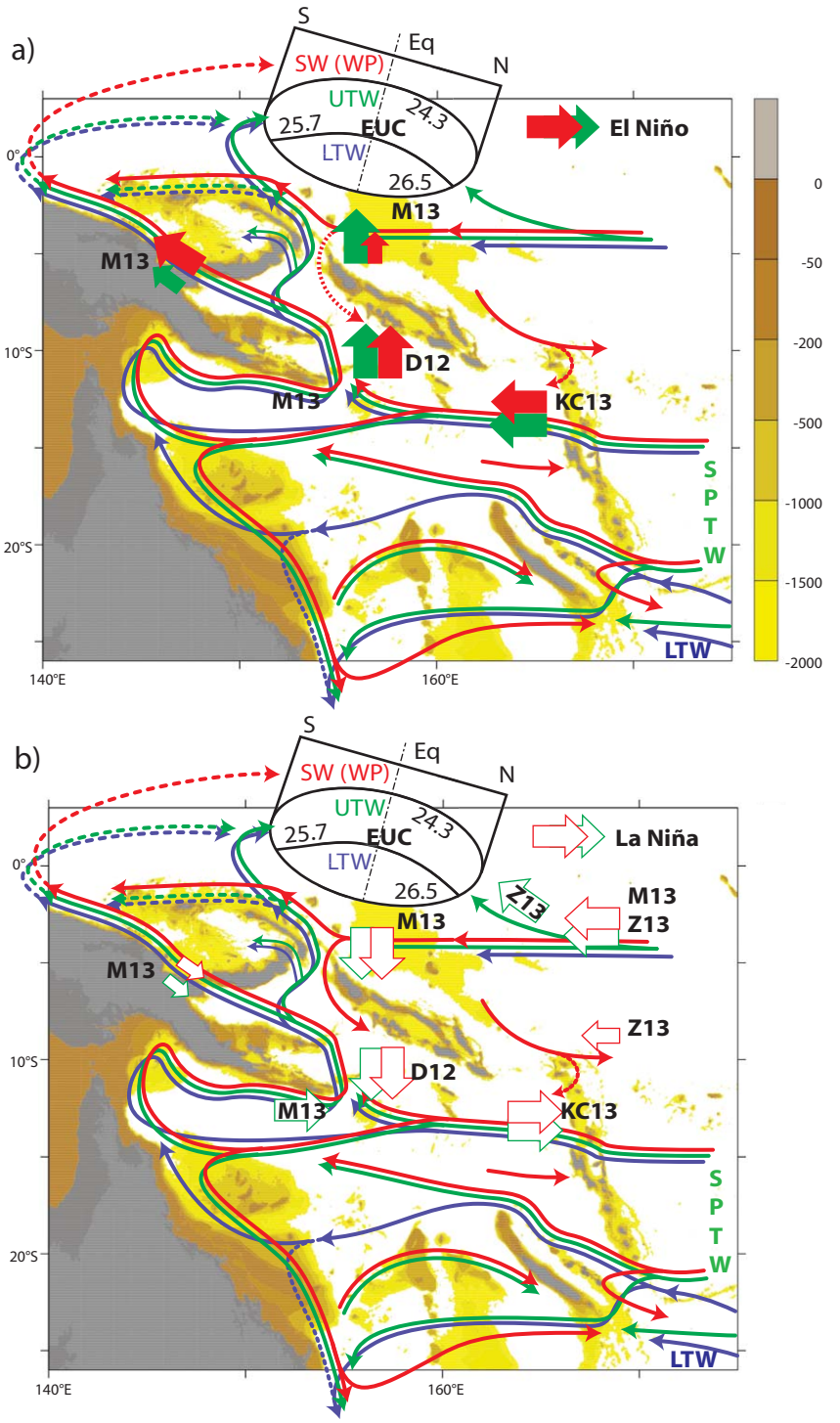

Figure 14. Water pathways and interannual variations. In both panels, continuous arrows denote pathways for the Surface Water (SW, red), UTW (green), and LTW (blue). The upper inset on each plot schematically indicates a meridional section across the EUC with the repartition of the water masses as they reach the equator. Large arrows indicate the main anomalies that are generated during (a) El Niño events and (b) La Niña events. The absence of arrow indicate no clear influence (e.g. regarding LTW). The interannual variations refer to *Melet et al.* [2013] (M13); *Kessler and Cravatte* [2013a] (KC13); *Zilberman et al.* [2013] (Z13); *Davis et al.* [2012] (D12); The mean flow pathways were established based on observations with references given in Appendix A (Figure A1).

the pathway from Vitiaz Strait to the central part of the EUC is relatively long and complex, the derivation through the Solomon Strait cause thermocline waters to join the equator in a faster way. Solomon Sea water flowing equatorward through Solomon Strait join SEC waters flowing westward east of the Solomon

Islands to form the NICU and feed predominantly the southern and shallower portion of the EUC. In contrast, the lower and central portions of the EUC essentially come from the Vitiaz pathway [inset of Figure 14a; *Melet et al*., 2010a; *Grenier et al*., 2011].

Numerical simulations suggest that 50% of the UTW that ultimately joins the equator flows through the LLWBCs, with the remaining 50% using interior pathways [*Qu et al*., 2013]. The Southwest Pacific UTW pathways are indicated by the green arrows on Figure 14a: a northern branch flows east of the Solomon Islands and New Ireland (in the NICU), whereas the other part enters the Coral Sea (mainly in the NVJ) and the Solomon Sea (in the NGCU) before exiting through all three Solomon Sea straits.

During El Niño events, the NVJ increases at the entrance of the Coral Sea (Figure 14a, large green arrows). At UTW level, observations and models show that the transport directly enters the Solomon Sea and joins the NGCU. Numerical simulations suggest that UTW transport is limited in Vitiaz Strait and the increase is mostly felt in Solomon Strait so that the positive anomaly joins the EUC through a shorter pathway. In the surface layer, the Vitiaz Strait transport increases during El Niño because of less dynamical limitation of transport in that depth-range (Figure 14a, large red arrows and references). Numerical simulations also show that the perturbation is asymmetric during La Niña events (Figure 14b): the anomalous decrease in the NVJ supply to the Coral Sea (large empty arrows) comes with a decrease in the NGCU which impacts both surface and thermocline waters in Solomon Strait with little change in the Vitiaz Strait.

LTW (blue arrows on Figure 14a) forms the lower part of the EUC and enters the equatorial region predominantly through the deep LLWBCs [*Qu et al*., 2009]. LTW enters the Coral Sea mostly in the NCJ, then flows through the GPC before entering the Solomon Sea [*Kessler and Cravatte*, 2013a; *Grenier et al*., 2013]. Numerical simulations suggest that LTW that ultimately joins the EUC mostly flows through the Vitiaz pathway [*Grenier et al*., 2011]; however, the fate of Vitiaz LTW that does not ultimately join the EUC is not precisely understood.

The interannual variability of this LTW pathway is different from that of UTW. *Davis et al*. [2012] show that, in the LTW depth range, the NGCU variability is not correlated with ENSO. In the Coral Sea, *Kessler and Cravatte* [2013a] suggested that the NVJ is essentially correlated with ENSO, while the NCJ is not. Therefore, the longer NCJ-GPC-NGCU pathway is less correlated with ENSO, and its variability remains undocumented.

4.4.2. Equatorward Heat Transports and Spiciness Anomalies

The increasing coverage of Argo data allowed detection of the large-scale UTW spiciness anomalies that are formed during winter in the southeastern subtropical gyre [*Kolodziejczyk and Gaillard*, 2012]. These anomalies undergo isopycnal and diapycnal mixing along the various water pathways [*Qu et al*., 2013] and appear to be significantly diminished before they reach the equator. Both diapycnal and isopycnal mixing seems particularly active in the Solomon Sea, as suggested by a model incorporating a tidal-mixing scheme [*Melet et al*., 2011] and the high energy found at submesoscales (subsection 5.4.1). Diapycnal mixing could also occur downstream of the Solomon Sea Straits as in the *Grenier et al*. [2011] numerical simulation and/or in the EUC as suggested by the small vertical scales found there [*Richards et al*., 2012]. In addition to small-scale mixing, the large-scale anomalies advect, or propagate westward with a speed that depends on latitude (i.e., presence of a jet or Rossby wave), so that the resulting patterns tend to loose their initial shape with lagged anomalies reaching the LLWBCs or/and the equator depending on pathways.

This strong damping of spiciness anomalies therefore precludes simple tracking of advective or propagating patterns through the Southwest Pacific region to assess their influence on equatorial conditions, as suggested by earlier numerical experiments [*Giese*, 2002; *Yeager and Large*, 2004; *Luo et al*., 2005; *Nonaka and Sasaki*, 2007]. Nevertheless, the SPICE results confirm the importance of the South Pacific LLWBC transport variations in the warm pool (and warm water volume) and EUC mass and heat budget. LLWBC transports generally increase with El Niño (Figure 14a), and counterbalance interior-driven changes in western equatorial Pacific warm water volume (subsection 4.3) [*Lengaigne et al*., 2012]. The resulting interannual anomalies of equatorward heat fluxes, which can vary by a factor of two between extreme El Niño and La Niña conditions [*Melet et al*., 2013], are therefore dominated by transport variations [e.g., *Kleeman et al*., 1999] rather than temperature or salinity anomalies.

In the *surface* layer, salinity is modified during the transit through the Solomon and Bismarck Seas by the heavy rainfall, river runoff, and upwelling systems. This modification is time-dependent, with strong seasonal and ENSO influence [*Delcroix et al*., 2014].

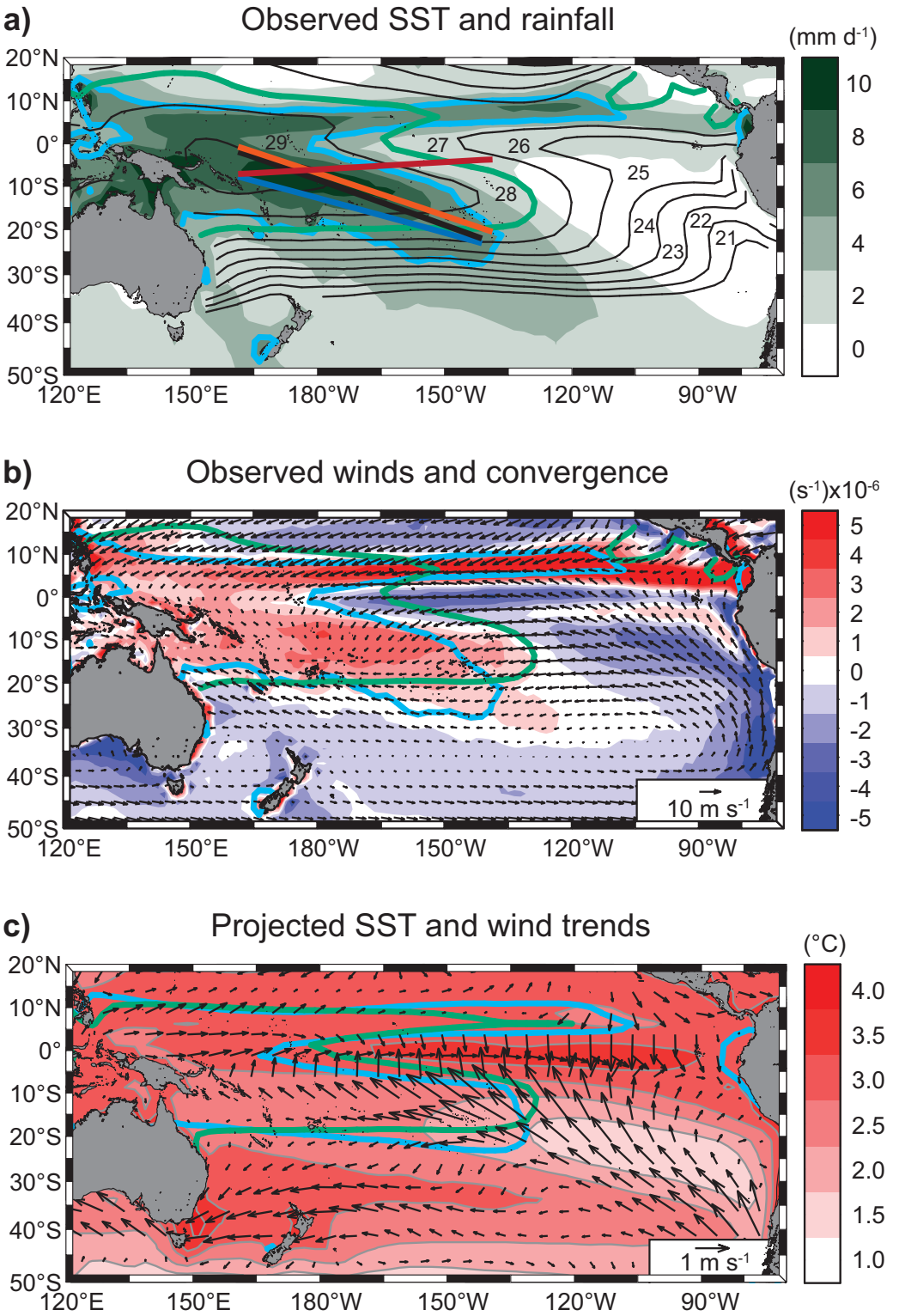

Figure 15. Observed climatology (1981–2005) and projected climate change (2074–2098 minus 1981–2005) during the peak season for the SPCZ; austral summer (December–February). (a) NOAA SST (°C, contours and labels) and GPCP rainfall (mm d^{-1}, color scale). SST contour interval: 1°C; starting at 20.5°C. Green contours depict the warm pool (27.5°C isotherm) and blue contours enclose the SPCZ (5 mm d^{-1} average rainfall), throughout. The SPCZ position for La Niña (blue), neutral (black), moderate El Niño (orange), and zonal events (red) is superimposed; as in *Vincent et al*. [2011]. (b) ERA-interim 10 m winds (vectors) and convergence (s^{-1}, color scale). (c) CMIP5 multimodel (31) mean projections of SST (color scale) and near-surface winds (vectors) for the 8.5 W m^{-2} representative concentration pathway. Green and blue contours enclose, respectively, the simulated warm pool and SPCZ during 1981–2005.

4.4.3. Poleward Pathways

Large variability of the poleward transport has been demonstrated to occur at all depths in numerical models [*Schiller et al*., 2008]. *van Sebille et al*. [2012] showed a large interannual variability in the TO, but not over longer time scales. Over longer time scales, the supergyre acceleration/enhanced EAC extension and its influence on temperature and salinity around Tasmania (subsection 4.2) directly affects the local biodiversity [*Ridgway*, 2007; *Suthers et al*., 2011; *Johnson et al*., 2011]. While the supergyre acceleration is caused by wind changes, the repercussions on global climate are unknown [*Cai*, 2006].

The subtropical front in the southern Tasman Sea near New Zealand extends south to nearly 50°S before following a convoluted path (subsection 4.2) south of New Zealand. Here it turns sharply to hug the east coast of the South Island and finally joins the TF/EAUC waters [Figure 4; *Smith et al*., 2013]. Whereas subtropical water from the Tasman Sea is lost along this path, the total flow that leaves the Tasman Sea via this route is small, but persistent; estimated at 1 Sv from hydrographic sections off the southeastern coast of New Zealand [*Sutton*, 2001]. The subtropical temperature, the strength of the front and the eddy activity have been increasing over the past decades in the confluence of the subtropical and subantarctic currents east of New Zealand in response to increasing wind stress curl over the basin [*Fernandez et al*., 2014].

4.5. SPCZ

The SPCZ is the largest rainband in the Southern Hemisphere with rain rates exceeding 5 mm d^{-1} on average during austral summer (Figure 15a). As the SPCZ forms the eastern boundary of the SPICE field programs (Figure 3), study of atmosphere interactions with regional ocean circulations have been conducted through remote sensing and climate modeling of the SPCZ formation and variability.

Regional SST gradients determine the near surface wind structure (Figure 15b) that supports SPCZ-related moisture convergence in observations [*Lintner and Neelin*, 2008] and climate models [*Niznik and Lintner*, 2013]. This SST dependence was also found in mid-Holocene numerical simulations, with different orbital forcing and SST pattern resulting in a shifted SPCZ [*Mantsis et al*., 2013]. Nevertheless, the SST distribution being itself related to the wind, SST/wind/rainfall all adjust together to determine the tilted SPCZ, so that no single parameter can be simply isolated [*Takahashi and Battisti*, 2007]. Heaviest rainfall associated with the SPCZ (Figure 15a, black line) is typically located poleward of the meridional SST gradient (i.e., between the warm pool and cooler equatorial waters [Figure 15b; *Cai et al*., 2012; *Widlansky et al*., 2012]) in a region of converging trade winds.

The tilted orientation of the SPCZ is partly explained by the zonal SST and surface pressure gradients extending from poleward of the heaviest rainfall in the western Pacific to the cooler waters and higher pressures in the eastern Pacific [*Widlansky et al*., 2010]. In the subtropics, synoptic disturbances propagate from south of Australia into the central South Pacific where upper troposphere mean westerly winds decelerate and wave energy density accumulates; thereby supporting convection which forms the diagonal component of the rain band [*Widlansky et al*., 2010; *Matthews*, 2012]. Centered over much cooler waters to the east, the Pacific subtropical high acts as the eastern boundary of the SPCZ [*Takahashi and Battisti*, 2007].

On interannual timescales, four typical structures of the SPCZ position were identified by *Vincent et al*. [2011] (Figure 15a, colored lines); each influenced by the slowly varying SST and wind patterns associated with ENSO. During extreme El Niño events, such as 1997/1998, the SPCZ becomes nearly zonal (red line) as the meridional SST gradient vanishes between the equator and 15°S.

5. SPICE Legacy

In the preceding sections, we discussed operations that are ongoing as a continuation of SPICE. Some studies are still exploratory whereas others are oriented toward long-term monitoring. In this section, we list the achievements of these studies and then discuss remaining questions and new research directions.

5.1. Major Achievements

One of the main motivations for SPICE was to determine whether changes in either LLWBC temperature or transport matter to climate (section 1). We now have a much improved understanding of the region. Specifically, SPICE has lead to

1. A refined description of the oceanic pathways to the equator: Jets, WBCs, *direct* NVJ path to the Solomon Sea, and EUC water origins; as well as their seasonal and interannual variations;

2. The observation that equatorward spiciness anomalies are strongly damped in the LLWBC system, with the transport anomalies dominating the signals;
3. Discovery of the deep extension of the NCJ and GPC, versus the broad and shallow NVJ;
4. Unprecedented description on the Solomon Sea circulation, its inflows, outflows, and their partitions;
5. Discovery of the TF/EAC interplay and opposite variations on decadal timescales;
6. A much improved description of the TF outflow and circulation around northern New Zealand;
7. A much improved description of the EAC Extension, variability and impact on ocean conditions;
8. An improved understanding of the southeastward tilt of the SPCZ in relation with SST, wind and rainfall.

5.2. Ongoing Operations

Despite successful simulations and model-based analyses of ocean dynamics in the SPICE region, many numerical modeling challenges remain. Very high resolution (order 1/36°) nested regional simulations are presently analyzed, but the computational burden to run these at basin-scale and over multiple decades is still prohibitive. Other challenges include inaccurate or missing topography at high spatial resolution and lack of accurate multiscale coast-to-shelf to open-ocean subgrid-scale parameterization, for both vertical and horizontal mixing, including effects by tides and internal waves. Algorithms capable of such full parameterization are under active development.

The high variability seen in both the circulation and water properties [see *Kessler and Cravatte*, 2013b, Table 1] produces aliasing in point-wise measurements from cruises and gliders, suggesting that repeat measurements are needed. Monitoring of key currents and transports is ongoing: into the Coral Sea (HR-XBT, mooring and glider measurements across the ECC and SEC [*Maes et al*., 2011]); Tasman Sea transports through the HR-XBT "Tasman Box" [*Roemmich et al*., 2005], as well as the Brisbane-Yokohama line that crosses the Coral and Solomon Seas. In the Solomon Sea, two hydrographic surveys were completed and moorings have been deployed since 2012 in the Solomon Straits to provide direct observation of the outflows [*Eldin et al*., 2013].

The WBC transports through the Solomon Sea are monitored through moorings and repeat gliders, as well as the NQC/GPC off the GBR, whereas the EAC current-meter array measurements are still being pursued (subsection 5.3.3). In addition, Argo floats are released on a regular basis in the SPICE region (section 2).

Information about operations is available from the SPICE web site http://spiceclivar.org. These new measurements, along with the aforementioned very high-resolution simulations, will help better resolve the regional oceanic circulation and atmospheric affects, in the coming 2–3 years.

5.3. Unresolved SPICE Issues

5.3.1. Mixing

Temperature anomalies undergo significant damping along their pathways to the equator (subsection 4.4) and high latitudes. Two model studies identify the Solomon Sea and downstream as areas of strong mixing [*Melet et al*., 2011; *Grenier et al*., 2011], as do global simulations of internal wave activity [*Simmons et al*., 2004], however, in situ measurements are unavailable to verify these simulations. The potentially large mixing contribution from intense mesoscale and submesoscale activity in the Solomon Sea, as well as tidal forcing in the straits also needs to be quantified [section 5.4.1; *Gourdeau et al*., 2014; *Jackson et al*., 2012]. Mixing occurring on the edge of EAC eddies and at the Australian continental shelf due to internal wave energy dissipation is also under investigation (B. Sloyan, personal communication, 2014).

5.3.2. Coral Sea

The deep extent of the NCJ and GPC still needs to be better measured and understood. While the SEC and jets have been thoroughly documented at the entrance of the Coral Sea, three regions lack basic descriptions. The SCJ was not properly documented due to its subsurface nature, high level of eddy activity [*Qiu et al*., 2009], and priorities given to the documentation of other currents. The NCJ bifurcation region against Australia, as well as the GPC variability still lack documentation.

5.3.3. Tasman Sea

Understanding of the full-depth EAC property transport and its time variations is far from complete. We still lack a sustained time series of full-depth property observations of the boundary flow of the EAC across

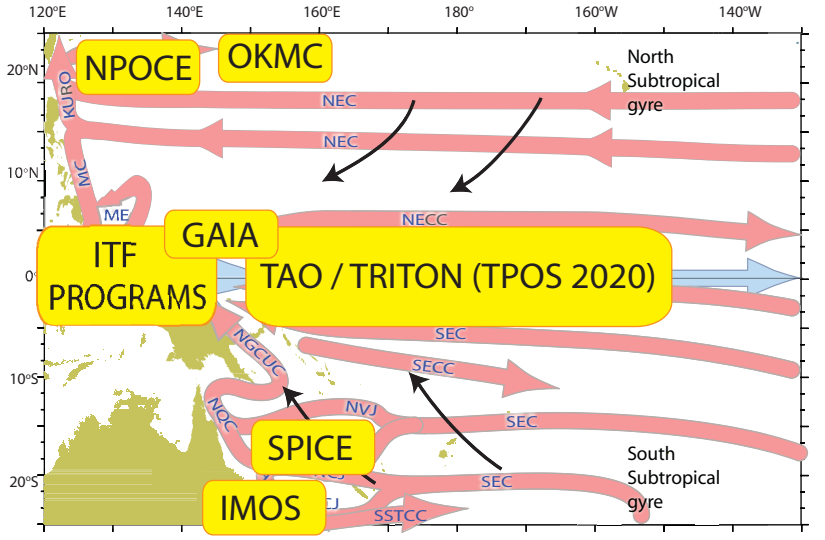

Figure 16. Concurrent CLIVAR programs in the western Pacific. With the equatorial TAO/TRITON/TPOS-2020 measurements (http://tpos2020.org), the Indonesian Throughflow (ITF Gateway; http://www.ldeo.columbia.edu/res/div/ocp/projects/SE_Asian_Archipelago), the Northwestern Pacific Ocean Circulation and Climate Experiment (*NPOCE*, http://npoce.qdio.ac.cn), Origins of the Kuroshio and Mindanao Currents (OKMC), Korea Institute of Ocean Science & Technology GAIA observations (http://eng.kiost.ac) and SPICE (http://spiceclivar.org), all oceanic pathways to the equator are being measured simultaneously.

its entire offshore extent that are of sufficient duration to resolve seasonal, interannnual, and decadal signals.

The complicated dynamics at the EAC separation point and the high eddy variability makes it challenging to design an appropriate monitoring array. A 2 year mooring array was maintained at 30°S [*Mata et al.*, 2000], but its limited width did not fully resolve the offshore edge of the EAC. Furthermore, its location within the most energetic portion of the EAC eddy field weakened the signal-to-noise ratio (Figure 7). A mooring array was deployed in 2012 in a more suitable location, 26°S, where the EAC is still coherent and its flow is relatively uniform with minimum variability and coincident with an HR-XBTs *Tasman Box* line (Figure 3). Initial analysis of the EAC mooring array indicates large transport variability (K. Ridgway and B. Sloyan, personal communication, 2014) and emphasizes the need for the long-term monitoring of the EAC. To fulfil this key observational requirement, redeployment of the IMOS EAC mooring array is planned for mid-2015.

5.3.4. Solomon Sea

The Solomon Sea circulation, water mass transformation, and strait transport partition are presently being measured (section 4.3, 5.2). In spite of new observations, three questions remain in the Solomon Sea: (1) Is there a WBC east of the Solomon Islands such as the SICU? (2) How much water is transported in the Indispensable Strait? (3) Is the interannual variability of the flow partition through the different straits similar to what models suggest? These questions will need to be addressed through further in situ measurements.

5.3.5. Link to the Equator and ENSO

Further investigation is needed to fully identify the main regions and mechanisms responsible for the damping of the subtropical anomalies along different water pathways (section 4.4) and how much is ultimately transmitted to the EUC. But the EUC is not the sole destination of the waters exiting the Solomon Sea, and the fate of the anomalies is unclear. For instance, some of the excess waters during an El Niño may feed the NECC, the EUC (which increases in the far west, but weakens over the central Pacific in the course of El Niño), or the Indonesian Throughflow. We know that the NGCU system contributes to the deep Indonesian Throughflow, but it remains unknown how much is contributed in the surface layer and how the pathways vary with ENSO. LLWBCs of the Northwest Pacific have also been the focus of CLIVAR programs, so that measurements are available north and south of the equator and through the Indonesian Throughflow quasi-simultaneously (Figure 16). Analysis of these adjacent observations will provide a more balanced budget of the equatorial waters supplies.

With these new advances, it will be timely to reassess the questions of the impact of the Southwest Pacific waters on ENSO, decadal variability and longer climate signals. Such questions include (1) Does refined

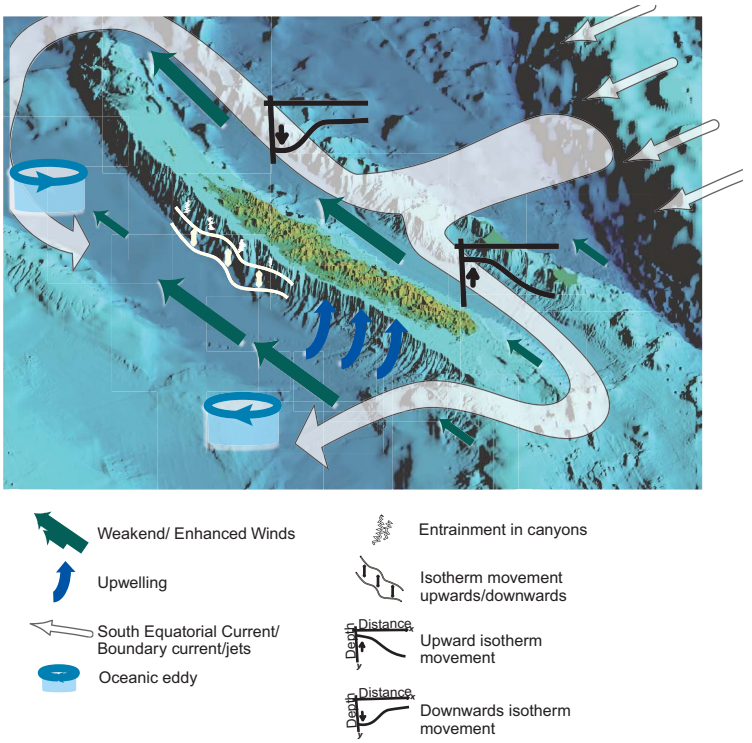

Figure 17. The four processes associated with islands that alter ocean circulation and nutrient supply, illustrated over the topography of New Caledonia. from *Ganachaud et al.* [2011].

modeling of the southern thermocline water inflow improve ENSO or decadal prediction? (2) Is monitoring important to ENSO prediction? These issues will need to be addressed using the newly available and developing observational platforms and high-resolution regional models combined with global coupled models.

5.3.6. Link to High Latitudes

The connection between the South Pacific and Indian oceans via the TO (subsection 4.2) varies due to different factors and an improved understanding of its variability and trend is important as it is a component of the global overturning circulation, modulating the global ocean heat and carbon budgets. Whereas the relationship with the TF has been established on decadal timescales, no link between the two systems has been determined at longer timescales. There is abundant evidence to show that the EAC Extension off Tasmania has increased over the past 60 years but the mechanism underlying this trend remains uncertain. For example, *Wu et al.* [2012] suggest that the EAC warming is due to an intensification of the current, whereas previous results indicate that there has been a poleward shift of the South Pacific winds and EAC system within a related poleward displacement of the gyre core [*Cai et al.*, 2005]. In contrast, the WBCs and their confluence east of New Zealand (which is the gyre western boundary at these latitudes) show higher temperatures and increased eddy activities, but no southward displacement [*Fernandez et al.*, 2014].

5.4. Future Developments and New Questions

5.4.1. Submesoscale Processes

The present high-resolution numerical simulations point to exceptionally large variability in the Solomon Sea related to mesoscale eddies [*Gourdeau et al.*, 2014; *Hristova et al.*, 2014]. The Solomon Sea was used as a regional "modeling laboratory," because of its specific configuration with tides, islands, and WBCs (subsection 4.3). The submesoscale permitting resolution (section 3) is now providing access to new and rich information, with possible consequences on horizontal and vertical mixing. The discovery of this part of the energy spectrum lead to exploring new approaches of image data assimilation, strongly motivated by the prospects of the SWOT satellite (a NASA/CNES project that will provide map of the sea surface topography at submesoscale resolution over the satellite swath extension) [*Gaultier et al.*, 2014]. The submesoscale features were also observed in surface salinity observations in the Coral Sea [*Maes et al.*, 2013], leading hopefully to new research foci.

5.4.2. Southwest Pacific and Climate Change

Whereas large uncertainties remain among climate models regarding the ENSO and the SPCZ responses to climate change [*Collins et al*., 2010; *Brown et al*., 2013b], the majority of future projections suggest faster warming along the equator compared to the SPCZ region (Figure 15c). The changing SST pattern is likely to enhance equatorial convection [*Ma et al*., 2012], strengthen southeasterly trade winds, and weaken meridional SST gradients [*Xie et al*., 2010], potentially leading to moisture divergence and future drying in parts of the SPCZ [*Widlansky et al*., 2012]. The uneven future warming of the tropical Pacific may almost double the frequency of "zonal-SPCZ" events (Figure 15a; red line), possibly shifting the mean rainfall pattern equatorward [*Cai et al*., 2012; *Widlansky et al*., 2012], with direct consequences on freshwater resources in the Pacific islands.

Projected changes to the wind strength and direction in the South Pacific will affect Southwest Pacific currents. To the south, high-resolution regional models embedded in global climate simulations project increased transport in the EAC Extension during the 21st century [*Sun et al*., 2012; *Oliver and Holbrook*, 2014a]. Similarly, direct examination of CMIP projections suggests future increase in the NGCU transport toward the equator [*Sen Gupta et al*., 2012], with foreseeable changes in the thermocline structure and water properties. Together, these simulations suggest likely future impacts on ENSO dynamics and equatorial ecosystems.

Many questions remain open regarding the effect of anthropogenic forcing, such as: (a) is the multidecadal extension of the EAC attributable to anthropogenic climate change? (b) how warm is the southwest Tasman Sea hotspot likely to reach in the future given the change in dynamics? (c) what are the likely effects of extreme upper ocean temperatures on marine ecological communities [e.g., *Oliver et al*., 2014] and in particular, on benthic communities that are not mobile? (d) what is the best approach to effectively downscale projected ocean temperature changes in the Tasman Sea to the shelf and coastal domain [e.g., *Oliver and Holbrook*, 2014b]? (e) is Tasman Sea net primary productivity likely to increase or decrease due to the associated dynamical effects of the EAC extension under climate change [e.g., *Matear et al*., 2013]? Similar challenges and questions are applicable to the equatorial region.

5.4.3. Toward Coastal and Island Scales

Islands in the Southwest Pacific region are particularly sensitive to climate variability and the oceanic environment. Over the past 20 years, sea level around the SPICE region has risen at over three times the global average rate [*Meyssignac et al*., 2012] and the ocean acidification combined with ocean warming could jeopardize coral growth toward the middle of this century or even before [*Veron et al*., 2009]. Clearly, sustainable development in the region must incorporate adaptation to climate variability and change.

Island sea level, SST and climate are controlled by the ocean via both basin-scale conditions and local processes. Drought and flooding events are often related to ENSO conditions and the associated location and intensity of the SPCZ [e.g., *Murphy et al*., 2014], which also influences sea level variability [*Widlansky et al*., 2014]. Furthermore, the ocean conditions control local temperature and air-sea fluxes, tropical cyclone intensity, and trajectories, transports of fish larvae as well as steric sea level.

SPICE has led to new measurements and modeling of the Southwest Pacific. Numerical simulations and ocean assimilation products are more accurate, providing improved boundary conditions to high-resolution models on island scales. Coastal and island processes add to large-scale conditions in various ways (Figure 17), specific to each place (see, e.g., *Schiller et al*. [2009b] regarding the GBR; *Ganachaud et al*. [2010]; *Lefevre et al*. [2010]; *Marchesiello et al*. [2010]; *Fuchs et al*. [2012] S. Cravatte et al., Regional circulation around New Caledonia from two decades of observations, submitted to *Journal of Marine System*., 2014, regarding the island of New Caledonia). Specific investigations are needed to understand and anticipate how large scale conditions affect local conditions.

Appendix A: References for Circulation Pathways

Figure A1 indicates the different references that were used to draw the circulation pathways of Fig. 14.

Appendix B: Acronyms

AGRIF	Adaptative Grid Refinement In Fortran
ADCP	Acoustic Doppler Current Profiler

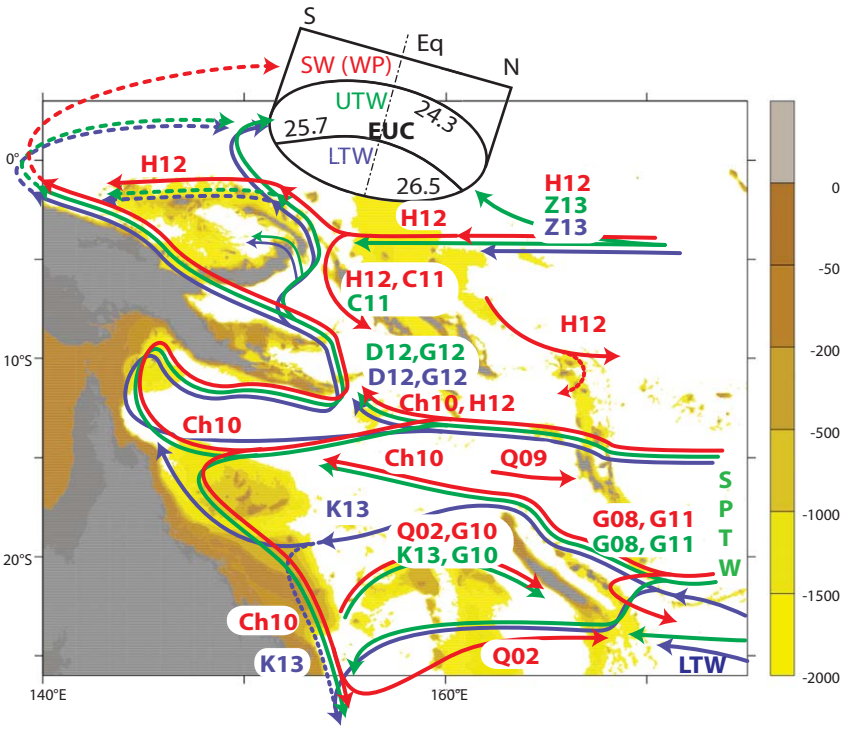

Figure A1. Water mass pathways from observations. Continuous arrows denote the Surface Water (SW, red), Upper Thermocline Water (UTW, green) and Lower Thermocline Water (LTW, blue), with both UTW and LTW. The upper inset on each panel indicates schematically a meridional section across the EUC with the repartition of the water masses upon reaching the equator. The references describing these pathways based on *observations* are given as follow: *Qu and Lindstrom* [2002] (Q02); *Ganachaud et al.* [2008b] (G08); *Ridgway et al.* [2008] (R08); *Qiu et al.* [2009] (Q09); *Choukroun et al.* [2010] (Ch10); *Ganachaud et al.* [2010] (G10); *Cravatte et al.* [2011] (C11); *Gasparin et al.* [2011] (G11); *Gasparin et al.* [2012] (G12); *Hristova and Kessler* [2012] (H12); *Davis et al.* [2012] (D12); *Kessler and Cravatte* [2013a] (KC13); *Zilberman et al.* [2013] (Z13); and *Sutton and Bowen* [2014] (S13).

BRAN	Bluelink ocean ReANalysis
CSSC	Coral Sea Counter Current
EAC	East Australia Current
EAUC	East Auckland Current
ECC	East Caledonian Current
ENSO	El Niño Southern Oscillation
FBCC	Fiji Basin Counter Current
GBR	Great Barrier Reef
GBRUC	Great Barrier Reef Undercurrent
GPC	Gulf of Papua Current
HR-XBT	High Resolution eXpendable BathyThermograph
IMOS	Integrated Marine Observing System
LLWBC	Low Latitude Western Boundary Currents
LTW	Lower Thermocline Water
NBCU	New Britain Coastal Undercurrent
NCJ	North Caledonian Jet
NGCU	New Guinea Coastal Undercurrent
NICU	New Ireland Coastal Undercurrent
NQC	North Queensland Current
NVJ	North Vanuatu Jet
PIES	Pressure Inverted EchoSounder
Q-IMOS	Queensland node of the Integrated Marine Observing System
SCJ	South Caledonian Jet
SEC	South Equatorial Current

SECC	South Equatorial Counter Current
SICU	Solomon Island Coastal Undercurrent (hypothetical)
SGU	Saint George Undercurrent
SPCZ	South Pacific Convergence Zone
SPTW	South Pacific Tropical Water
SST	Sea Surface Temperature
STCC	South Pacific Subtropical Counter Current
STMW	Subtropical Mode Waters
SW	Surface Water
TF	Tasman Front
TO	Tasman Outflow
UTW	Upper Thermocline Water
WBC	Western Boundary Currents

Acknowledgments

SPICE is a contribution to the CLIVAR and GEOTRACES International programs. This review involves many more scientists who contributed indirectly. We are grateful to the ship crews who made possible the various in situ measurements. The collaboration of SOPAC/SPC, PI-GOOS, and the different Pacific Island countries that are involved is greatly appreciated. The accomplishments were made possible through concurrent contributions of national funding agencies. Those include ANR project ANR-09-BLAN-0233-01 and INSU/LEFE projects IMAGO and CYBER. The CNES provided support to some numerical simulations. BMS and KR where supported by the Australian Climate Change Science Program jointly funded by the Department of the Environment and CSIRO. Australia's Integrated Marine Observing System (IMOS) is funded by the Australian Governments National Collaborative Research Infrastructure Strategy, the Super Science Initiative and, regarding Queensland-IMOS, the Queensland State Government. Operations and numerical experiments were also made possible through NSF and NOAA funding. We thank the two anonymous reviewers whose remarks greatly helped to improve the manuscript.

References

Berkelmans, R., S. J. Weeks, and C. R. Steinberg (2010), Upwelling linked to warm summers and bleaching on the great barrier reef, *Limnol. Oceanogr.*, *55*, 2634–2644.

Blanke, B., and S. Raynaud (1997), Kinematics of the pacific equatorial undercurrent: An Eulerian and Lagrangian approach from GCM results, *J. Phys. Oceanogr.*, *27*(6), 1038–1053, doi:10.1175/1520-0485(1997)027<1038:KOTPEU>2.0.CO;2.

Bowen, M. M., J. L. Wilkin, and W. J. Emery (2005), Variability and forcing of the east Australian current, *J. Geophys. Res.*, *110*, C03019, doi:10.1029/2004JC002533.

Brassington, G. B., N. Summons, and R. Lumpkin (2011), Observed and simulated Lagrangian and eddy characteristics of the east Australian current and the Tasman sea, *Deep Sea Res., Part II*, *58*(5), 559–573, doi:10.1016/j.dsr2.2010.10.001.

Brown, J. N., A. Sen Gupta, J. R. Brown, L. C. Muir, J. S. Risbey, P. Whetton, X. Zhang, A. Ganachaud, B. Murphy, and S. E. Wijffels (2013a), Implications of CMIP3 model biases and uncertainties for climate projections in the western tropical pacific, *Clim. Change*, *119*, 147–161, doi:10.1007/s10584-012-0603-5.

Brown, J. R., S. B. Power, F. P. Delage, R. A. Colman, A. F. Moise, and B. F. Murphy (2011), Evaluation of the south pacific convergence zone in IPCC AR4 climate model simulations of the twentieth century, *J. Clim.*, *24*(6), 1565–1582, doi:10.1175/2010JCLI3942.1.

Brown, J. R., A. F. Moise, and R. A. Colman (2013b), The south pacific convergence zone in CMIP5 simulations of historical and future climate, *Clim. Dyn.*, *41*, 2179–2197, doi:10.1007/s00382-012-1591-x.

Burrage, D. (1993), Coral sea currents, *Corella*, *17*(5), 135–145.

Cai, W. (2006), Antarctic ozone depletion causes an intensification of the southern ocean super-gyre circulation, *Geophys. Res. Lett.*, *33*, L03712, doi:10.1029/2005GL024911.

Cai, W., G. Shi, T. Cowan, D. Bi, and J. Ribbe (2005), The response of the southern annular mode, the east Australian current, and the southern mid-latitude ocean circulation to global warming, *Geophys. Res. Lett.*, *32*, L23706, doi:10.1029/2005GL024701.

Cai, W., et al. (2012), More extreme swings of the south pacific convergence zone due to greenhouse warming, *Nature*, *488*(7411), 365–369, doi:10.1038/nature11358.

Choukroun, S., P. V. Ridd, R. Brinkman, and L. I. W. McKinna (2010), On the surface circulation in the western coral sea and residence times in the great barrier reef, *J. Geophys. Res.*, *115*, C06013, doi:10.1029/2009JC005761.

Church, J. A., and F. M. Boland (1983), A permanent undercurrent adjacent to the great barrier reef, *J. Phys. Oceanogr.*, *13*(9), 1747–1749, doi:10.1175/1520-0485(1983)013<1747:APUATT>2.0.CO;2.

Collins, M., et al. (2010), The impact of global warming on the tropical pacific ocean and el nino, *Nat. Geosci.*, *3*(6), 391–397, doi:10.1038/ngeo868.

Couvelard, X., P. Marchesiello, L. Gourdeau, and J. Lefevre (2008), Barotropic zonal jets induced by islands in the southwest pacific, *J. Phys. Oceanogr.*, *38*(10), 2185–2204, doi:10.1175/2008JPO3903.1.

Cravatte, S., A. Ganachaud, Q.-P. Duong, W. S. Kessler, G. Eldin, and P. Dutrieux (2011), Observed circulation in the Solomon sea from SADCP data, *Prog. Oceanogr.*, *88*(1-4), 116–130, doi:10.1016/j.pocean.2010.12.015.

Davis, R. E., W. S. Kessler, and J. T. Sherman (2012), Gliders measure western boundary current transport from the south pacific to the equator, *J. Phys. Oceanogr.*, *42*(11), 2001–2013, doi:10.1175/JPO-D-12-022.1.

De'ath, G., K. E. Fabricius, H. Sweatman, and M. Puotinen (2012), The 27–year decline of coral cover on the great barrier reef and its causes, *Proc. Natl. Acad. Sci. U. S. A.*, *109*(44), 17,995–17,999, doi:10.1073/pnas.1208909109, PMID: 23027961.

Delcroix, T., M.-H. Radenac, S. Cravatte, G. Alory, L. Gourdeau, F. Leger, A. Singh, and D. Varillon (2014), Sea surface temperature and salinity seasonal changes in the western Solomon and Bismarck seas, *J. Geophys. Res. Oceans*, *119*, 2642–2657, doi:10.1002/2013JC009733.

Djath, B., A. Melet, J. Verron, J.-M. Molines, B. Barnier, L. Gourdeau, and L. Debreu (2014a), A 1/36 model of the Solomon sea embedded into a global ocean model: On the setting up of an interactive open boundary nested model system, *J. Oper. Oceanogr.*, *7*(1), 34–46.

Djath, B., J. Verron, A. Melet, L. Gourdeau, B. Barnier, and J. M. Molines (2014b), Multiscale analysis of dynamics from high resolution realistic model of the solomon sea, *J. Geophys. Res. Oceans*, *119*, 6286–6304, doi:10.1002/2013JC009695.

Eldin, G., A. Ganachaud, S. Cravatte, and C. Jeandel (2013), Pandora cruise provides an unprecedented description of the solomon sea, *CLIVAR Newsl. Exch.*, *61*(18), 24–25.

Everett, J. D., M. E. Baird, P. R. Oke, and I. M. Suthers (2012), An avenue of eddies: Quantifying the biophysical properties of mesoscale eddies in the tasman sea, *Geophys. Res. Lett.*, *39*, L16608, doi:10.1029/2012GL053091.

Fernandez, D., M. Bowen, and L. Carter (2014), Intensification and variability of the confluence of subtropical and subantarctic boundary currents east of New Zealand, *J. Geophys. Res. Oceans*, *119*, 1146–1160, doi:10.1002/2013JC009153.

Fine, R. A., R. Lukas, F. M. Bingham, M. J. Warner, and R. H. Gammon (1994), The western equatorial pacific: A water mass crossroads, *J. Geophys. Res.*, *99*(C12), 25,063–25,080, doi:10.1029/94JC02277.

Fuchs, R., C. Dupouy, P. Douillet, M. Caillaud, A. Mangin, and C. Pinazo (2012), Modeling the impact of a la nina event on a south west pacific lagoon, *Mar. Pollut. Bull.*, *64*, 1596–1613, doi:10.1016/j.marpolbul.2012.05.016.

Ganachaud, A., et al. (2007), Southwest pacific ocean circulation and climate experiment (SPICE). Part 1: Scientific background, CLIVAR Publ. Ser., vol. 111, NOAA/CLIVAR. [Available at http://clivar.org.]

Ganachaud, A., et al. (2008a), Southwest Pacific ocean circulation and climate experiment (SPICE): Part 2. Implementation plan, *CLIVAR Publ. Ser*. vol. 133, NOAA/CLIVAR. [Available at http://clivar.org.]

Ganachaud, A., L. Gourdeau, and W. Kessler (2008b), Bifurcation of the subtropical south equatorial current against New Caledonia in December 2004 from a hydrographic inverse box model, *J. Phys. Oceanogr.*, *38*(9), 2072–2084, doi:10.1175/2008JPO3901.1.

Ganachaud, A., A. Vega, M. Rodier, C. Dupouy, C. Maes, P. Marchesiello, G. Eldin, K. Ridgway, and R. Le Borgne (2010), Observed impact of upwelling events on water properties and biological activity off the southwest coast of New Caledonia, *Mar. Pollut. Bull.*, *61*(7-12), 449–464.

Ganachaud, A., et al. (2011), Observed and expected changes to the tropical pacific ocean, in *Vulnerability of Tropical Pacific Fisheries and Aquaculture to Climate Change*, edited by J. Bell, J. Johnson, and A. Hobday, pp. 101–187, Secr. of the Pac. Comm., Noumea.

Gasparin, F., A. Ganachaud, and C. Maes (2011), A western boundary current east of New Caledonia: Observed characteristics, *Deep Sea Res., Part I*, *58*(9), 956–969, doi:10.1016/j.dsr.2011.05.007.

Gasparin, F., A. Ganachaud, C. Maes, F. Marin, and G. Eldin (2012), Oceanic transports through the Solomon sea: The bend of the New Guinea coastal undercurrent, *Geophys. Res. Lett.*, *39*, L15608, doi:10.1029/2012GL052575.

Gasparin, F., C. Maes, J. Sudre, V. Garcon, and A. Ganachaud (2014), Water mass analysis of the Coral Sea through an Optimum Multiparameter method, *J. Geophy. Res.*, doi:10.1002/2014JC010246.

Gaultier, L., B. Djath, J. Verron, A. Melet, J.-M. Brankart, and P. Brasseur (2014), Assessing the feasibility of the inversion of sub-mesoscales in a high-resolution Solomon sea model, *J. Geophys. Res. Oceans*, *119*, 4520–4541, doi:10.1002/2013JC009660.

Giese, B. S. (2002), Southern hemisphere origins of the 1976 climate shift, *Geophys. Res. Lett.*, *29*(2), 2002, doi:10.1029/2001GL013268.

Godfrey, J. S. (1989), A sverdrup model of the depth-integrated flow for the world ocean allowing for island circulations, *Geophys. Astrophys. Fluid Dyn.*, *45*(1-2), 89–112, doi:10.1080/03091928908208894.

Goni, G., et. al. (2010), The Ship of Opportunity Program, in *Proceedings of OceanObs'09: Sustained Ocean Observations and Information for Society*, vol. 2, pp. 366–383, Eur. Space Agency, ESA Publication WPP-306, doi:10.5270/OceanObs09.cwp.35. [Available at http://www.oceanobs09.net.]

Gourdeau, L., W. S. Kessler, R. E. Davis, J. Sherman, C. Maes, and E. Kestenare (2008), Zonal jets entering the coral sea, *J. Phys. Oceanogr.*, *38*(3), 715–725, doi:10.1175/2007JPO3780.1.

Gourdeau, L., J. Verron, A. Melet, W. Kessler, F. Marin, and B. Djath (2014), Exploring the mesoscale activity in the solomon sea: A complementary approach with a numerical model and altimetric data, *J. Geophys. Res. Oceans*, *119*, 2290–2311, doi:10.1002/2013JC009614.

Grenier, M., S. Cravatte, B. Blanke, C. Menkes, A. Koch-Larrouy, F. Durand, A. Melet, and C. Jeandel (2011), From the western boundary currents to the pacific equatorial undercurrent: Modeled pathways and water mass evolutions, *J. Geophys. Res.*, *116*, C12044, doi:10.1029/2011JC007477.

Grenier, M., C. Jeandel, F. Lacan, D. Vance, C. Venchiarutti, A. Cros, and S. Cravatte (2013), From the subtropics to the central equatorial pacific ocean: Neodymium isotopic composition and rare earth element concentration variations, *J. Geophys. Res. Oceans*, *118*, 592–618, doi:10.1029/2012JC008239.

Grenier, M., C. Jeandel, and S. Cravatte (2014), From the subtropicss to the equator in the southwest pacific: Continental material fluxes quantified using neodymium parameters along modeled thermocline water pathways, *J. Geophys. Res. Oceans*, *119*, 3948–3966, doi:10.1002/2013JC009670.

Gu, D., and S. G. Philander (1997), Interdecadal climate fluctuations that depend on exchanges between the tropics and extratropics, *Science*, *275*(5301), 805–807, doi:10.1126/science.275.5301.805.

Hartin, C. A., R. A. Fine, B. M. Sloyan, L. D. Talley, T. K. Chereskin, and J. Happell (2011), Formation rates of subantarctic mode water and antarctic intermediate water within the south pacific, *Deep Sea Res., Part I*, *58*(5), 524–534, doi:10.1016/j.dsr.2011.02.010.

Hasson, A., T. Delcroix, and J. Boutin (2013), Formation and variability of the south pacific sea surface salinity maximum in recent decades, *J. Geophys. Res. Oceans*, *118*, 5109–5116, doi:10.1002/jgrc.20367.

Hill, K. L., S. R. Rintoul, K. R. Ridgway, and P. R. Oke (2011), Decadal changes in the south pacific western boundary current system revealed in observations and ocean state estimates, *J. Geophys. Res.*, *116*, C01009, doi:10.1029/2009JC005926.

Holbrook, N. J., and N. L. Bindoff (1997), Interannual and decadal temperature variability in the southwest Pacific ocean between 1955 and 1988, *J. Clim.*, *10*(5), 1035–1049, doi:10.1175/1520-0442(1997)010<1035:IADTVI>2.0.CO;2.

Holbrook, N. J., and N. L. Bindoff (1999), Seasonal temperature variability in the upper southwest pacific ocean, *J. Phys. Oceanogr.*, *29*(3), 366–381, doi:10.1175/1520-0485(1999)029<0366:STVITU>2.0.CO;2.

Holbrook, N. J., and A. M. Maharaj (2008), Southwest pacific subtropical mode water: A climatology, *Prog. Oceanogr.*, *77*(4), 298–315, doi:10.1016/j.pocean.2007.01.015.

Holbrook, N. J., P. S.-L. Chan, and S. A. Venegas (2005a), Oscillatory and propagating modes of temperature variability at the 3-3.5- and 4-4.5-yr time scales in the upper southwest Pacific ocean, *J. Clim.*, *18*(5), 719–736.

Holbrook, N., P. Chan, and S. Venegas (2005b), CORRIGENDUM oscillatory and propagating modes of temperature variability at the 3-3.5- and 4-4.5-yr time scales in the upper southwest Pacific ocean, *J. Clim.*, *18*(10), 1637–1639.

Holbrook, N. J., I. D. Goodwin, S. McGregor, E. Molina, and S. B. Power (2011), ENSO to multi-decadal time scale changes in east Australian current transports and fort Denison sea level: Oceanic Rossby waves as the connecting mechanism, *Deep Sea Res., Part II*, *58*(5), 547–558, doi:10.1016/j.dsr2.2010.06.007.

Hristova, H. G., and W. S. Kessler (2012), Surface circulation in the Solomon Sea derived from Lagrangian drifter observations, *J. Phys. Oceanogr.*, *42*(3), 448–458, doi:10.1175/JPO-D-11-099.1.

Hristova, H. G., W. Kessler, J. C. McWilliams, and M. J. Molemaker (2014), Mesoscale variability and its seasonal variability in the solomon and coral seas, *J. Geophys. Res. Oceans*, *119*, 4669–4687, doi:10.1002/2013JC009741.

Jackson, C., J. da Silva, and G. Jeans (2012), The generation of nonlinear internal waves, *Oceanography*, *25*(2), 108–123, doi:10.5670/oceanog.2012.46.

Johnson, C. R., et al. (2011), Climate change cascades: Shifts in oceanography, species' ranges and subtidal marine community dynamics in eastern Tasmania, *J. Exp. Mar. Biol. Ecol.*, *400*(1-2), 17–32, doi:10.1016/j.jembe.2011.02.032.

Kessler, W. S., and S. Cravatte (2013a), Mean circulation of the coral sea, *J. Geophys. Res. Oceans*, *118*, 6385–6410, doi:10.1002/2013JC009117.

Kessler, W. S., and S. Cravatte (2013b), ENSO and short-term variability of the south equatorial current entering the coral sea, *J. Phys. Oceanogr.*, *43*, 956–969, doi:10.1175/JPO-D-12-0113.1.
Kessler, W. S., and L. Gourdeau (2007), The annual cycle of circulation of the southwest subtropical pacific, analyzed in an ocean GCM, *J. Phys. Oceanogr.*, *37*(6), 1610–1627, doi:10.1175/JPO3046.1.
Kleeman, R., J. P. McCreary, and B. A. Klinger (1999), A mechanism for generating ENSO decadal variability, *Geophys. Res. Lett.*, *26*(12), 1743–1746, doi:10.1029/1999GL900352.
Koch-Larrouy, A., G. Madec, P. Bouruet-Aubertot, T. Gerkema, L. Bessires, and R. Molcard (2007), On the transformation of pacific water into Indonesian through flow water by internal tidal mixing, *Geophys. Res. Lett.*, *34*, L04604, doi:10.1029/2006GL028405.
Kolodziejczyk, N., and F. Gaillard (2012), Observation of spiciness interannual variability in the pacific pycnocline, *J. Geophys. Res.*, *117*, C12018, doi:10.1029/2012JC008365.
Lee, T., and I. Fukumori (2003), Interannual-to-decadal variations of Tropical–Subtropical exchange in the Pacific ocean: Boundary versus interior pycnocline transports, *J. Clim.*, *16*(24), 4022–4042, doi:10.1175/1520-0442(2003)016<4022:IVOTEI>2.0.CO;2.
Lefevre, J., P. Marchesiello, N. C. Jourdain, C. Menkes, and A. Leroy (2010), Weather regimes and orographic circulation around New Caledonia, *Mar. Pollut. Bull.*, *61*(7-12), 413–431, doi:10.1016/j.marpolbul.2010.06.012.
Lengaigne, M., U. Hausmann, G. Madec, C. Menkes, J. Vialard, and J. M. Molines (2012), Mechanisms controlling warm water volume interannual variations in the equatorial pacific: Diabatic versus adiabatic processes, *Clim. Dyn.*, *38*(5-6), 1031–1046, doi:10.1007/s00382-011-1051-z.
Lintner, B. R., and J. D. Neelin (2008), Eastern margin variability of the south pacific convergence zone, *Geophys. Res. Lett*, *35*, L16701, doi:10.1029/2008GL034298.
Luo, Y., L. M. Rothstein, R.-H. Zhang, and A. Busalacchi (2005), On the connection between south pacific subtropical spiciness anomalies and decadal equatorial variability in an ocean general circulation model, *J. Geophys. Res.*, *110*, C10002, doi:10.1029/2004JC002655.
Ma, J., S.-P. Xie, and Y. Kosaka (2012), Mechanisms for tropical tropospheric circulation change in response to global warming, *J. Clim.*, *25*(8), 2979–2994, doi:10.1175/JCLI-D-11-00048.1.
Maes, C., L. Gourdeau, X. Couvelard, and A. Ganachaud (2007), What are the origins of the antarctic intermediate waters transported by the north Caledonian jet?, *Geophys. Res. Lett.*, *34*, L21608, doi:10.1029/2007GL031546.
Maes, C., D. Varillon, A. Ganachaud, F. Gasparin, L. Gourdeau, and F. Durand (2011), Geostrophic component of oceanic jets entering in the eastern coral sea observed with high-resolution XBT surveys (2008–2010), *Coriolis Mercator Ocean Q. Newsl.*, *41*, 25–32.
Maes, C., B. Dewitte, J. Sudre, V. Garcon, and D. Varillon (2013), Small-scale features of temperature and salinity surface fields in the Coral sea, *J. Geophys. Res. Oceans*, *118*, 5426–5438, doi:10.1002/jgrc.20344.
Mantsis, D. F., B. R. Lintner, A. J. Broccoli, and M. Khodri (2013), Mechanisms of mid-holocene precipitation change in the south pacific convergence zone, *J. Clim.*, *26*, 6937–6953, doi:10.1175/JCLI-D-12-00674.1.
Marchesiello, P., J. Lefevre, A. Vega, X. Couvelard, and C. Menkes (2010), Coastal upwelling, circulation and heat balance around New Caledonia's barrier reef, *Mar. Pollut. Bull.*, *61*(7-12), 432–448, doi:10.1016/j.marpolbul.2010.06.043.
Mata, M. M., M. Tomczak, S. Wijffels, and J. A. Church (2000), East Australian current volume transports at 30S: Estimates from the world ocean circulation experiment hydrographic sections PR11/P6 and the PCM3 current meter array, *J. Geophys. Res.*, *105*(C12), 28,509–28,526, doi:200010.1029/1999JC000121.
Matear, R. J., M. A. Chamberlain, C. Sun, and M. Feng (2013), Climate change projection of the Tasman sea from an eddy-resolving ocean model, *J. Geophys. Res. Oceans*, *118*, 2961–2976, doi:10.1002/jgrc.20202.
Matthews, A. J. (2012), A multiscale framework for the origin and variability of the south pacific convergence zone, *Q. J. R. Meteorol. Soc.*, *138*(666), 1165–1178, doi:10.1002/qj.1870.
McCreary, J. P., and P. Lu (1994), Interaction between the subtropical and equatorial ocean circulations: The subtropical cell, *J. Phys. Oceanogr.*, *24*(2), 466–497, doi:10.1175/1520-0485(1994)024<0466:IBTSAE>2.0.CO;2.
McGregor, S., N. J. Holbrook, and S. B. Power (2007), Interdecadal sea surface temperature variability in the equatorial pacific ocean. Part i: The role of off-equatorial wind stresses and oceanic Rossby waves, *J. Clim.*, *20*(11), 2643–2658, doi:10.1175/JCLI4145.1.
McGregor, S., N. J. Holbrook, and S. B. Power (2008), Interdecadal sea surface temperature variability in the equatorial pacific ocean. Part II: The role of Equatorial/Off-Equatorial wind stresses in a hybrid coupled model, *J. Clim.*, *21*(17), 4242–4256, doi:10.1175/2008JCLI2057.1.
McGregor, S., A. Sen Gupta, N. J. Holbrook, and S. B. Power (2009a), The modulation of ENSO variability in CCSM3 by extratropical Rossby waves, *J. Clim.*, *22*(22), 5839–5853, doi:10.1175/2009JCLI2922.1.
McGregor, S., N. J. Holbrook, and S. B. Power (2009b), The response of a stochastically forced ENSO model to observed off-equatorial wind stress forcing, *J. Clim.*, *22*(10), 2512–2525, doi:10.1175/2008JCLI2387.1.
McPhaden, M. J., and D. Zhang (2002), Slowdown of the meridional overturning circulation in the upper pacific ocean, *Nature*, *415*(6872), 603–608.
Melet, A., L. Gourdeau, W. S. Kessler, J. Verron, and J.-M. Molines (2010a), Thermocline circulation in the Solomon sea: A modeling study, *J. Phys. Oceanogr.*, *40*(6), 1302–1319, doi:10.1175/2009JPO4264.1.
Melet, A., L. Gourdeau, and J. Verron (2010b), Variability in Solomon sea circulation derived from altimeter sea level data, *Ocean Dyn.*, *60*(4), 883–900, doi:10.1007/s10236-010-0302-6.
Melet, A., J. Verron, L. Gourdeau, and A. Koch-Larrouy (2011), Equatorward pathways of Solomon sea water masses and their modifications, *J. Phys. Oceanogr.*, *41*, 810–826, doi:10.1175/2010JPO4559.1.
Melet, A., J. Verron, and J.-M. Brankart (2012), Potential outcomes of glider data assimilation in the Solomon sea: Control of the water mass properties and parameter estimation, *J. Mar. Syst.*, *94*, 232–246, doi:10.1016/j.jmarsys.2011.12.003.
Melet, A., L. Gourdeau, J. Verron, and B. Djath (2013), Solomon sea circulation and water mass modifications: Response at ENSO timescales, *Ocean Dyn.*, *63*(1), 1–19, doi:10.1007/s10236-012-0582-0.
Meyssignac, B., D. Salas y Melia, M. Becker, W. Llovel, and A. Cazenave (2012), Tropical pacific spatial trend patterns in observed sea level: Internal variability and/or anthropogenic signature?, *Clim. Past*, *8*(2), 787–802, doi:10.5194/cp-8-787-2012.
Murphy, B. F., S. B. Power, and S. McGree (2014), The varied impacts of El Nino Southern Oscillation on Pacific Island climates, *J. Clim.*, *27*(11), 4015–4036, doi:10.1175/JCLI-D-13-00130.1.
Niznik, M. J., and B. R. Lintner (2013), Circulation, moisture, and precipitation relationships along the south pacific convergence zone in reanalyses and CMIP5 models, *J. Clim.*, *26*, 10174–10192, doi:10.1175/JCLI-D-13-00263.1.
Nonaka, M., and H. Sasaki (2007), Formation mechanism for isopycnal Temperature-Salinity anomalies propagating from the eastern south pacific to the equatorial region, *J. Clim.*, *20*(7), 1305–1315, doi:10.1175/JCLI4065.1.
Oke, P. R., and D. A. Griffin (2011), The cold-core eddy and strong upwelling off the coast of new south wales in early 2007, *Deep Sea Res. Part II*, *58*(5), 574–591, doi:10.1016/j.dsr2.2010.06.006.

Oke, P. R., G. Brassington, J. Cumming, M. Martin, and F. Hernandez (2012), GODAE inter-comparisons in the tasman and coral seas, *J. Oper. Oceanogr.*, *5*(2), 11–24.

Oke, P. R., P. Sakov, M. L. Cahill, J. R. Dunn, R. Fiedler, D. A. Griffin, J. V. Mansbridge, K. R. Ridgway, and A. Schiller (2013), Towards a dynamically balanced eddy-resolving ocean reanalysis: BRAN3, *Ocean Model.*, *67*, 52–70, doi:10.1016/j.ocemod.2013.03.008.

Oliver, E. C. J., and N. J. Holbrook (2014a), Extending our understanding of south pacific gyre spin-up: Modeling the east Australian current in a future climate, *J. Geophys. Res. Oceans*, *119*, 2788–2805, doi:10.1002/2013JC009591.

Oliver, E. C. J., and N. J. Holbrook (2014b), A statistical method for improving continental shelf and nearshore marine climate predictions, *J. Atmos. Oceanic Technol.*, *31*(1), 216–232, doi:10.1175/JTECH-D-13-00052.1.

Oliver, E. C. J., S. J. Wotherspoon, M. A. Chamberlain, and N. J. Holbrook (2014), Projected tasman sea extremes in sea surface temperature through the twenty-first century, *J. Clim.*, *27*(5), 1980–1998, doi:10.1175/JCLI-D-13-00259.1.

Qiu, B., S. Chen, and W. S. Kessler (2009), Source of the 70-day mesoscale eddy variability in the coral sea and the north Fiji basin, *J. Phys. Oceanogr.*, *39*(2), 404–420, doi:10.1175/2008JPO3988.1.

Qu, T., and E. J. Lindstrom (2002), A climatological interpretation of the circulation in the western south pacific, *J. Phys. Oceanogr.*, *32*(9), 2492–2508, doi:10.1175/1520-0485-32.9.2492.

Qu, T., and E. J. Lindstrom (2004), Northward intrusion of antarctic intermediate water in the western pacific, *J. Phys. Oceanogr.*, *34*(9), 2104–2118, doi:10.1175/1520-0485(2004)034<2104:NIOAIW>2.0.CO;2.

Qu, T., S. Gao, I. Fukumori, R. A. Fine, and E. J. Lindstrom (2008), Subduction of south pacific waters, *Geophys. Res. Lett.*, *35*, L02610, doi:10.1029/2007GL032605.

Qu, T., S. Gao, I. Fukumori, R. A. Fine, and E. J. Lindstrom (2009), Origin and pathway of equatorial 13C water in the pacific identified by a simulated passive tracer and its adjoint, *J. Phys. Oceanogr.*, *39*(8), 1836–1853, doi:10.1175/2009JPO4045.1.

Qu, T., S. Gao, and R. A. Fine (2013), Subduction of south pacific tropical water and its equatorward pathways as shown by a simulated passive tracer, *J. Phys. Oceanogr.*, *43*(8), 1551–1565, doi:10.1175/JPO-D-12-0180.1.

Richards, K. J., Y. Kashino, A. Natarov, and E. Firing (2012), Mixing in the western equatorial pacific and its modulation by ENSO, *Geophys. Res. Lett.*, *39*, L02604, doi:10.1029/2011GL050439.

Ridgway, K., and J. R. Dunn (2003), Mesoscale structure of the mean east Australian current system and its relationship with topography, *Prog. Oceanogr.*, *56*(2), 189–222, doi:10.1016/S0079-6611(03)00004-1.

Ridgway, K. R. (2007), Long-term trend and decadal variability of the southward penetration of the east Australian current, *Geophys. Res. Lett.*, *34*, L13613, doi:10.1029/2007GL030393.

Ridgway, K. R., and J. R. Dunn (2007), Observational evidence for a southern hemisphere oceanic supergyre, *Geophys. Res. Lett.*, *34*, L13612, doi:10.1029/2007GL030392.

Ridgway, K. R., and J. S. Godfrey (1997), Seasonal cycle of the east Australian current, *J. Geophys. Res.*, *102*(C10), 22,921–22,936, doi:10.1029/97JC00227.

Ridgway, K. R., J. R. Dunn, and J. L. Wilkin (2002), Ocean interpolation by four-dimensional weighted least squares–application to the waters around Australasia, *J. Atmos. Oceanic Technol.*, *19*(9), 1357–1375, doi:10.1175/1520-0426(2002)019<1357:OIBFDW>2.0.CO;2.

Ridgway, K. R., R. C. Coleman, R. J. Bailey, and P. Sutton (2008), Decadal variability of east Australian current transport inferred from repeated high-density XBT transects, a CTD survey and satellite altimetry, *J. Geophys. Res.*, *113*, C08039, doi:10.1029/2007JC004664.

Roemmich, D., J. Gilson, J. Willis, P. Sutton, and K. Ridgway (2005), Closing the time-varying mass and heat budgets for large ocean areas: The tasman box, *J. Clim.*, *18*(13), 2330–2343, doi:10.1175/JCLI3409.1.

Roemmich, D., J. Gilson, R. Davis, P. Sutton, S. Wijffels, and S. Riser (2007), Decadal spinup of the south pacific subtropical gyre, *J. Phys. Oceanogr.*, *37*(2), 162–173, doi:10.1175/JPO3004.1.

Sallee, J.-B., K. Speer, S. Rintoul, and S. Wijffels (2010), Southern ocean thermocline ventilation, *J. Phys. Oceanogr.*, *40*(3), 509–529, doi:10.1175/2009JPO4291.1.

Sasaki, Y. N., S. Minobe, N. Schneider, T. Kagimoto, M. Nonaka, and H. Sasaki (2008), Decadal sea level variability in the south pacific in a global eddy-resolving ocean model hindcast, *J. Phys. Oceanogr.*, *38*(8), 1731–1747, doi:10.1175/2007JPO3915.1.

Schiller, A., P. Oke, G. Brassington, M. Entel, R. Fiedler, D. Griffin, and J. Mansbridge (2008), Eddy-resolving ocean circulation in the Asian–Australian region inferred from an ocean reanalysis effort, *Prog. Oceanogr.*, *76*(3), 334–365, doi:10.1016/j.pocean.2008.01.003.

Schiller, A., G. Meyers, and N. R. Smith (2009a), Observing systems: Taming Australia's last frontier, *Bull. Am. Meteorol. Soc.*, *90*(4), 436–440, doi:10.1175/2008BAMS2610.1.

Schiller, A., K. R. Ridgway, C. R. Steinberg, and P. R. Oke (2009b), Dynamics of three anomalous SST events in the coral sea, *Geophys. Res. Lett.*, *36*, L06606, doi:10.1029/2008GL036997.

Sen Gupta, A., A. Ganachaud, S. McGregor, J. N. Brown, and L. C. Muir (2012), Drivers of the projected changes to the Pacific ocean equatorial circulation, *Geophys. Res. Lett*, *39*, L09605, doi:10.1029/2012GL051447.

Simmons, H. L., R. W. Hallberg, and B. K. Arbic (2004), Internal wave generation in a global baroclinic tide model, *Deep Sea Res., Part II*, *51*(25-26), 3043–3068, doi:10.1016/j.dsr2.2004.09.015.

Smith, R. O., R. Vennell, H. C. Bostock, and M. J. Williams (2013), Interaction of the subtropical front with topography around southern New Zealand, *Deep Sea Res., Part I*, *76*, 13–26, doi:10.1016/j.dsr.2013.02.007.

Speich, S., B. Blanke, P. de Vries, S. Drijfhout, K. Doos, A. Ganachaud, and R. Marsh (2002), Tasman leakage: A new route in the global ocean conveyor belt, *Geophys. Res. Lett.*, *29*(10), 2002, doi:10.1029/2001GL014586.

SPICE Community (2012), Naming a western boundary current from Australia to the Solomon Sea (Burrage D., Cravatte S., Dutrieux P., Hughes R., Kessler W., Ganachaud A., Melet, A., Steinberg, C. R. and Schiller, A.), *CLIVAR Newsl. Exch.*, *58*, 28.

Sprintall, J., D. Roemmich, B. Stanton, and R. Bailey (1995), Regional climate variability and ocean heat transport in the southwest Pacific ocean, *J. Geophys. Res.*, *100*(C8), 15,865, doi:10.1029/95JC01664.

Sun, C., M. Feng, R. J. Matear, M. A. Chamberlain, P. Craig, K. R. Ridgway, and A. Schiller (2012), Marine downscaling of a future climate scenario for Australian boundary currents, *J. Clim.*, *25*(8), 2947–2962, doi:10.1175/JCLI-D-11-00159.1.

Suthers, I. M., et al. (2011), The strengthening east Australian current, its eddies and biological effects: An introduction and overview, *Deep Sea Res., Part I*, *58*(5), 538–546, doi:10.1016/j.dsr2.2010.09.029.

Sutton, P. (2001), Detailed structure of the subtropical front over Chatham rise, east of New Zealand, *J. Geophys. Res.*, *106*(C12), 31,045–31,056, doi:10.1029/2000JC000562.

Sutton, P., and M. Bowen (2011), Currents off the west coast of northland, New Zealand, *N. Z. J. Mar. Freshwater Res.*, *45*(4), 609–624, doi:10.1080/00288330.2011.569729.

Sutton, P., M. Bowen, and D. Roemmich (2005), Decadal temperature changes in the Tasman sea, *N. Z. Mar. Freshwater Res.*, *39*, 1321–1329.

Sutton, P. J. H., and M. Bowen (2014), Flows in the Tasman front south of Norfolk island, *J. Geophys. Res. Oceans*, *119*, 3041–3053, doi:10.1002/2013JC009543.

Sutton, P. J. H., and D. Roemmich (2001), Ocean temperature climate off North-East New Zealand, *N. Z. J. Mar. Freshwater Res.*, *35*(3), 553–565, doi:10.1080/00288330.2001.9517022.

Takahashi, K., and D. S. Battisti (2007), Processes controlling the mean tropical pacific precipitation pattern. Part II: The SPCZ and the southeast pacific dry zone, *J. Clim.*, *20*(23), 5696–5706, doi:10.1175/2007JCLI1656.1.

Tilburg, C. E., H. E. Hurlburt, J. J. O'Brien, and J. F. Shriver (2001), The dynamics of the east Australian current system: The tasman front, the east Auckland current, and the east cape current, *J. Phys. Oceanogr.*, *31*(10), 2917–2943, doi:10.1175/1520-0485(2001)031<2917:TDOTEA>2.0.CO;2.

Tsubouchi, T., T. Suga, and K. Hanawa (2007), Three types of south pacific subtropical mode waters: Their relation to the large-scale circulation of the south pacific subtropical gyre and their temporal variability, *J. Phys. Oceanogr.*, *37*(10), 2478–2490, doi:10.1175/JPO3132.1.

van Sebille, E., M. H. England, J. D. Zika, and B. M. Sloyan (2012), Tasman leakage in a fine-resolution ocean model, *Geophys. Res. Lett.*, *39*, L06601, doi:10.1029/2012GL051004.

Veron, J., O. Hoegh-Guldberg, T. Lenton, J. Lough, D. Obura, P. Pearce-Kelly, C. Sheppard, M. Spalding, M. Stafford-Smith, and A. Rogers (2009), The coral reef crisis: The critical importance of <350 ppm CO2, *Mar. Pollut. Bull.*, *58*(10), 1428–1436, doi:10.1016/j.marpolbul.2009.09.009.

Vincent, E. M., M. Lengaigne, C. E. Menkes, N. C. Jourdain, P. Marchesiello, and G. Madec (2011), Interannual variability of the south pacific convergence zone and implications for tropical cyclone genesis, *Clim. Dyn.*, *36*, 1881–1896, doi:10.1007/s00382-009-0716-3.

Webb, D. J. (2000), Evidence for shallow zonal jets in the south equatorial current region of the southwest pacific, *J. Phys. Oceanogr.*, *30*(4), 706–720.

Widlansky, M. J., P. J. Webster, and C. D. Hoyos (2010), On the location and orientation of the south pacific convergence zone, *Clim. Dyn.*, *36*(3-4), 561–578, doi:10.1007/s00382-010-0871-6.

Widlansky, M. J., A. Timmermann, K. Stein, S. McGregor, N. Schneider, M. H. England, M. Lengaigne, and W. Cai (2012), Changes in South Pacific rainfall bands in a warming climate, *Nat. Clim. Change*, *3*, 417–423, doi:10.1038/nclimate1726.

Widlansky, M. J., A. Timmermann, S. McGregor, M. F. Stuecker, and W. Cai (2014), An interhemispheric tropical sea level seesaw due to El Niño Taimasa, *J. Clim.*, *27*(3), 1070–1081, doi:10.1175/JCLI-D-13-00276.1.

Wu, L., et al. (2012), Enhanced warming over the global subtropical western boundary currents, *Nat. Clim. Change*, *2*(3), 161–166, doi:10.1038/nclimate1353.

Xie, S.-P., C. Deser, G. A. Vecchi, J. Ma, H. Teng, and A. T. Wittenberg (2010), Global warming pattern formation: Sea surface temperature and rainfall, *J. Clim.*, *23*, 966–986, doi:10.1175/2009JCLI3329.1.

Yeager, S. G., and W. G. Large (2004), Late-winter generation of spiciness on subducted isopycnals, *J. Phys. Oceanogr.*, *34*(7), 1528–1547, doi:10.1175/1520-0485(2004)034<1528:LGOSOS>2.0.CO;2.

Zhang, C. (2001), Intraseasonal perturbations in sea surface temperatures of the equatorial eastern pacific and their association with the Madden–Julian oscillation, *J. Clim.*, *14*(6), 1309–1322, doi:10.1175/1520-0442(2001)014<1309:IPISST>2.0.CO;2.

Zhang, L., and T. Qu (2014), Low-frequency variability of south pacific tropical water from Argo: Zhang et al.; low frequency variability of SPTW, *Geophys. Res. Lett.*, *41*, 2441–2446, doi:10.1002/2014GL059490.

Zilberman, N. V., D. H. Roemmich, and S. T. Gille (2013), The mean and the time-variability of the shallow meridional overturning circulation in the tropical south pacific ocean, *J. Clim.*, *26*, 4069–4087, doi:10.1175/JCLI-D-12-00120.1.